MAKING MORE SENSITIVE DNA SENSORS USING GOLD NANOPARTICLES AND DNA-BASED AMPLIFICATION NETWORKS

by

Herbert M. Huttanus

A thesis

submitted in partial fulfillment

of the requirements for the degree of

Master of Science in Materials Science and Engineering

Boise State University

May 2014

BOISE STATE UNIVERSITY GRADUATE COLLEGE

DEFENSE COMMITTEE AND FINAL READING APPROVALS

of the thesis submitted by

Herbert M. Huttanus

Thesis Title: Making More Sensitive DNA Sensors Using Gold Nanoparticles and DNA-Based Amplification Networks.

Date of Final Oral Examination: 26 March 2014

The following individuals read and discussed the thesis submitted by student Herbert M. Huttanus and they evaluated his presentation and response to questions during the final oral examination. They found that the student passed the final oral examination.

Jeunghoon Lee, Ph.D.	Chair, Supervisory Committee
William L. Hughes, Ph.D.	Member, Supervisory Committee
Bernard Yurke, Ph.D.	Member, Supervisory Committee

The final reading approval of the thesis was granted by Jeunghoon Lee, Ph.D., Chair of the Supervisory Committee. The thesis was approved for the Graduate College by John R. Pelton, Ph.D., Dean of the Graduate College.

ABSTRACT

This study focuses on the use of gold nanoparticles with DNA-based signal amplification as a detection method for low concentrations of DNA biomarkers.

Biotechnology is a rapidly evolving field with primarily medical applications. Early detection is a challenging process for some cancers and other diseases yet is so critical to successful treatment. Increasingly sensitive detection techniques are being developed, but the current gold standard for detecting nucleotide biomarkers at low concentrations is polymerase chain reaction. While this technique is sensitive, it requires the use of active enzymes, a thermocycler, and trained personnel working in a clean environment, and is thus not very feasible for diagnosing diseases in remote locations or third world epidemic scenarios. Gold nanoparticles with complimentary DNA probes provide an easy, colorimetric method for detecting a DNA target, but are not very sensitive to sub-nanomolar concentrations without post-hybridization enhancement or sensitive instruments. To overcome this limitation, we employ enzyme-free, DNA-based amplification networks that use cascading hybridization reactions to produce multiple nanoparticle binding events per molecule of target DNA. Our data show that the DNA-based amplification does increase sensitivity of our colorimetric gold nanoparticles without sacrificing their ease of use. We also expand this detection method to other biomolecule of interest, by using an aptamer sequence to bind a small biomolecule and then trigger the DNA-based amplification network.

TABLE OF CONTENTS

LIST OF TABLES

LIST OF FIGURES

LIST OF ABBREVIATIONS

Ade	Adenosine
Apt	Aptamer
CHA	Catalytic Hairpin Assembly
DNA	Deoxyribo Nucleic Acid
HCR	Hybridization Chain Reaction
H,T,L,S	Hairpin, Target, Linker or Signal strands respectively
LSPR	Localized Surface Plasmon Resonance
NP	Nanoparticle
PCR	Polymerase Chain Reaction
PBS	Phosphate Buffered Saline
SDS	Sodium Dodecyl Sulfate
SPR	Surface Plasmon Resonance
TMSD	Toehold Mediated Strand Displacement
Trn	Transducer

CHAPTER ONE: CHALLENGE, TOOLS AND POSSIBILITIES

Introduction

There is a growing demand for simple, sensitive, and inexpensive biological assays for detecting low concentrations of clinically relevant molecular markers such as micro RNAs and other nucleic acids [1-3]. Common methods for nucleic acid sensing include using fluorescent dyes and polymerase chain reactions [4, 5]. These common methods require sensitive enzymes or photosensitive dyes as well as expensive laboratory equipment, which is not always available at point of care nor is it field deployable. Because they are not field deployable, they are not ideal for biomolecule detection at remote locations, such as pathogenic outbreaks in a third world country or field studies of the spread of genetically modified plants [6]. For such applications, a simpler test for the end user would be preferable and would have to meet several criteria. The testing method should be cheap, easy to employ, easy to read, durable, reliable and sensitive. The first three criteria, in particular, are best met by a colorimetric test such as the litmus test or a home pregnancy test. Simple colorimetric detection of many types of analytes can be achieved using gold nanoparticles (NPs) with appropriate functionalization [7-10].

Such colorimetric tests could be field deployable and made to be as simple to use as a home pregnancy test [11]. These tests utilize the unique optical properties of gold NPs, which are dependent on the size, shape, and inter-particle distance, the latter of which may be exploited by binding the particles together. Gold NP-based methods have

several advantages over alternatives such as fluorescent dyes in that (1) gold NPs have high extinction coefficients relative to organic dyes, which translate to a stronger signal, and (2) their color change can be detected without using external instrumentation. In addition, gold nanoparticles can be used to test for a wide variety of analytes by coating the nanoparticles with appropriate ligands. This study focuses on using DNA probes attached to a nanoparticle surface in order to detect a specific DNA sequence. Understanding the application of gold nanoparticles for diagnostics requires both an understanding and characterization of their unique optical properties.

What Is the Plasmon?

Gold nanoparticles have absorption spectrum very different from that of bulk gold because of surface plasmon resonance. A surface plasmon is a semi-quantized oscillation of a plasma of free electrons [12]. The electron plasma in question is a collection of valence electrons in the gold. These electrons are delocalized and only weakly held by the nuclei of metal atoms. When an electric field is applied to a closed system, the electrons will shift towards the higher potential. A force is also applied to the nucleus and to the inner shell electrons, but the mass of the nucleus, and the partial charge cancellation from the inner shell electrons limit displacement. The displacement of the plasma is uniform throughout most of a bulk material but at the material surfaces on the high potential side, electrons accumulate, and the reverse happens on the low potential surface where electron density is reduced. This establishes a dipole [13].

If the electric field is removed, the dipole's electric field supplies a restoring force that sends the valence electrons back toward the positive pole. This restoring force overcorrects (as many restoring forces do) and establishes an oscillation of the dipole.

Dipole oscillation is quickly dampened in semiconductors, but in metals with high conductivity, the oscillation is preserved. The frequency of the dipole oscillation is largely determined by the material properties, but also by the distance between the poles and thus by nanoparticle size [14].

When a sinusoidal electric field is applied (i.e., electromagnetic radiation), it is possible for the external electric field to be either in phase or out of phase with the particle's intrinsic frequency of dipole oscillation. When the external field oscillates at the right frequency and is in phase with the dipole oscillation, the photon is said to resonate with the particle and is thus absorbed by the metal to establish a plasmon (Fig. 1.1). This dipole description is an oversimplification since quadripole and other high order modes of oscillation have been observed for the bulk valence electrons. The important thing to remember, however, is that the wavelength of light that can be absorbed or scattered by the nanoparticle is dependent on the material properties, size, and the geometry of the plasmonic particle.

The mode most responsible for the color of gold nanoparticles is actually the surface plasmon. Unlike the bulk plasmon described previously, the surface plasmon is a resonance of electric potential across a barrier between substances. In the case of gold nanoparticles, the barrier is the nanoparticle surface where metallic gold and the suspending solution meet [15]. Just as before, the valence electrons can be considered to exist as fluid plasma. Surface plasmons exist when the absorption of light triggers the propagation of a wave of electrons along the plasmonic barrier. If the gold surface were large and flat, the wave would spread, but when confined to a nano-scale spherical

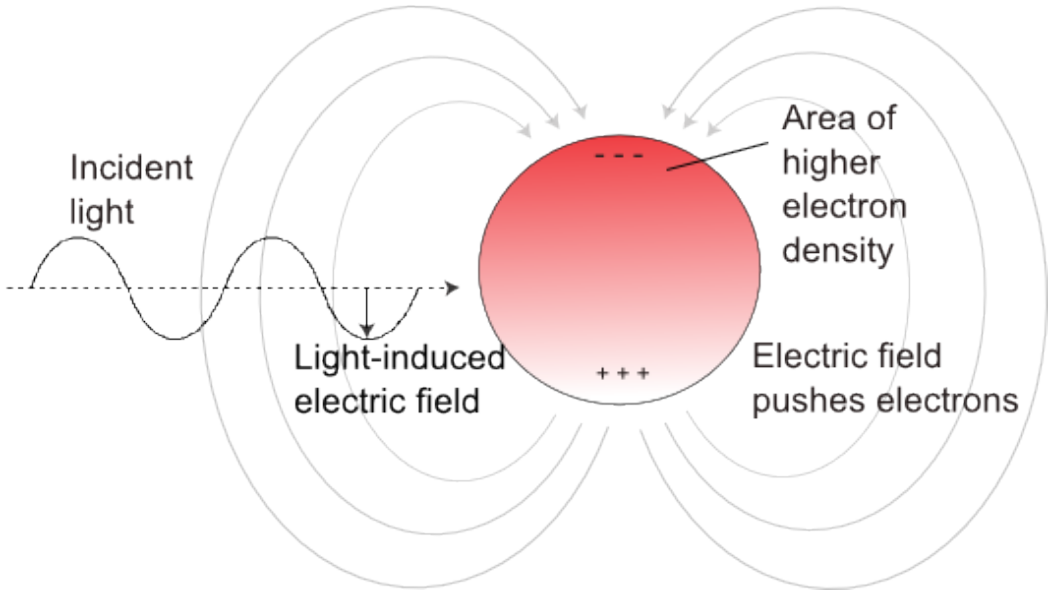

Figure 1.1 The Displacement of Nanoparticle Electrons by an Electromagnetic Field. An external electric field can bias the metallic valence electrons towards one end of the nanoparticle, creating a dipole. The energy in a photon's oscillating electric field will be absorbed by the particle if the frequency matches that of the nanoparticle's inherent dipole flipping frequency.

surface, the wave has the opportunity to become a standing wave, should the wavelength of the excitation source match that of the nanoparticle's resonant surface plasmon wavelength. In such quantized scenarios, the surface plasmon is localized and the oscillation is termed local surface plasmon resonance (LSPR) [16].

Plasmon Coupling

The absorption of light by metallic nanoparticles via LSPR is interesting, but by itself offers little more practical application than rendering a colloidal suspension of metal nanoparticle a different color than the bulk metal. Most of the interesting applications involving metal nanoparticles deal with the coupling between LSPRs or to other electronic systems.

Recall that oscillating dipoles are established by the surface plasmon. Since dipoles create an electric field around themselves, then surface plasmons have an oscillating electric field that could be affecting or affected by the electric fields of nearby surface plasmons [14]. The model needed to describe such interactions will depend on the number of surface plasmon resonances involved. One plasmon is difficult enough to model with the Maxwell equations and two can be much more complicated [17], but three body equations and higher order interactions require a great deal of simplifying assumptions.

While solving the two particle equation is more like solving the one particle equation in many respects, it turns out that the need to do this only arises in very particular applications of nanoparticles, where discrete numbers of particles are being brought together on some engineered nanostructure. The vast majority of nanoparticle applications, however, involve the more random aggregation of nanoparticles, which brings nanoparticles from a dilute solution into dense aggregates either by a chemical change in their stability or by using bridging molecules attached to the particle surface, such as DNA [18, 19]. The shift in state from dilute to aggregated particles drastically changes the degree of particle coupling and the final optical properties of the nanoparticles. By engineering these solutions to aggregate under a controllable trigger, they can be used as sensors or switch-able optical systems.

In general, the absorption spectra of the aggregates red-shift with respect to the dilute systems, meaning that the coupled plasmon resonances are of lower energy [20]. Using this feature, researchers can design assays in which the analyte will aggregate the particles and change the color of the solution from red to blue [13]. Mathematical models

exist for the plasmon frequency's dependence on nanoparticle size and proximity to other particles, but a truly detailed investigation of the resonance models is outside of the scope for this study. The relationship between nanoparticles size and spectrum was taken instead from empirical data [21] and the degree of plasmonic shift upon coupling was used only qualitatively based on the principals described in this section.

Application of Nanoparticles

Now that we know what surface plasmon resonances are and how they couple, we can use this information to describe their use in a bio-sensing application. Gold nanoparticles are a popular choice due to their chemical stability and strong extinction coefficient compared to many organic dyes. Gold nanoparticle-based assays work by triggered aggregation. The nanoparticles are coated with ligands for the analyte of interest and, as multiple ligands bind to the same analyte, multiple gold nanoparticles are brought together around the analyte causing plasmon coupling and a visible color change (Figure 1.2). If the target analyte is DNA, the appropriate ligand is a complimentary DNA strand. Such DNA sensors were pioneered by Elghanian *et al.* [7]. In his seminal design, the probe solution contains a combination of two nanoparticles. Both nanoparticles are gold spheres of the same diameter, but they have been functionalized with different DNA probes. The DNA is attached by using chemically modified synthetic DNA that contains a terminal thiol group. The thiol group readily binds to gold surfaces and the attached DNA, which is negatively charged, improves the nanoparticle solubility.

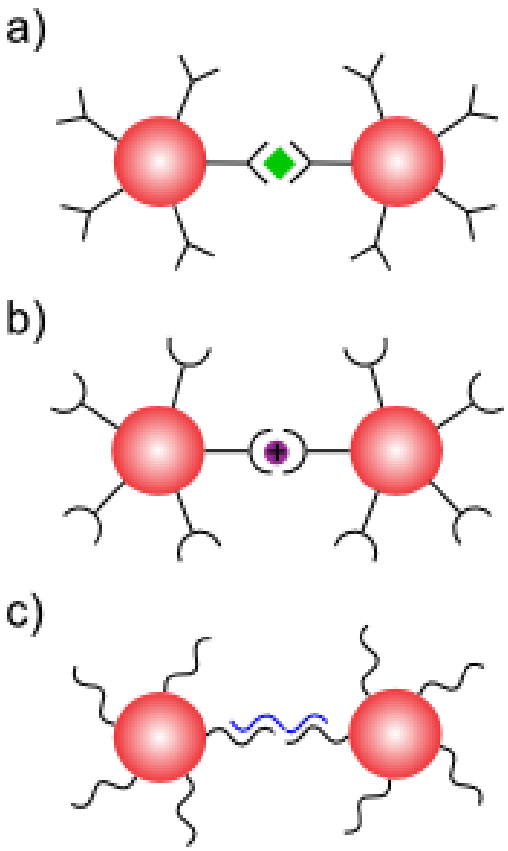

Figure 1.2 Nanoparticles Coated with Ligands. In nanoparticle-based assays, the nanoparticle surfaces are coated with ligands for the analyte. a) If the analyte is a protein, the ligand may be an antibody. As two antibodies bind to the same protein, two nanoparticles are linked together into plasmon coupling range. If the protein does not have multiple binding sites for the same antibody, two different antibodies can be used, and half the nanoparticles will use one type of antibody while the other half use the other. antibody. b) Metal ions can be detected by using chelating agents on the nanoparticle surface. c) Sequence specific DNA detection is possible by using complimentary DNA probes on the surface of the nanoparticles. Similar to the case with antibodies, two different probe sequences are often necessary, each for a different portion of the target sequence. The ligands themselves are bound to the gold surface by chemical modification of the ligands that introduce a thiol group that has a natural affinity for gold.

The two different probe strands used are complimentary to a different half of the target DNA sequence. If the target sequence is present in the test, then it will hybridize to both probe sequences by standard Watson-Crick base pairing. Binding the probe strands together means binding two nanoparticles together such that they can couple, provided that the DNA bridge between them is of similar magnitude or smaller than the nanoparticle diameter (Fig. 1.3).

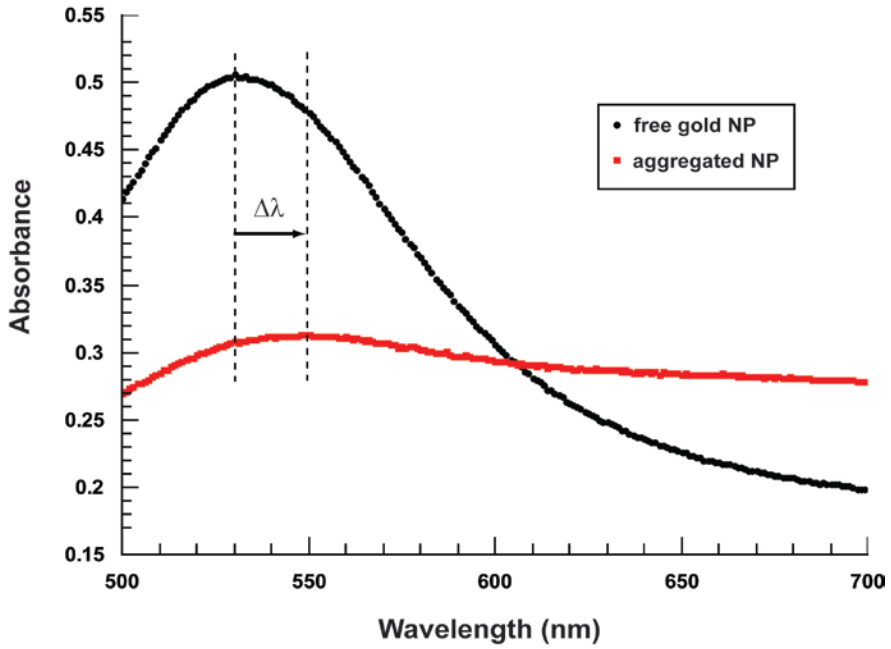

Figure 1.3 Aggregation-Induced Spectrum Shift. As the nanoparticles are brought close together by their mutual hybridization to the same target strand, their plasmons couple and their absorbance spectrum changes in three notable ways. First, the absorbance peak in the visible range shifts towards higher wavelengths since the coupled plasmons have a lower energy oscillation mode. Second, the peak is broadened because there exists a size distribution among the particles, and the opportunity to form different combinations of different sizes provides an even greater range of coupled plasmon frequencies. Finally, the peak is lowered partially due to the broadening and partially due to some aggregates becoming too large to establish plasmons effectively. Any of these three changes can be quantitatively measured as a qualitative metric for extent of aggregation. The combined affect makes the solution's visible color change from red to a more muted purple or blue.

At very low analyte concentrations, this would only create a few dimers not capable of altering the optical properties of the solution by much. Each nanoparticle, however, is coated with many such probe strands, and sufficiently high concentrations of the DNA analyte will bind each nanoparticle to multiple neighbors, forming a dense, three dimensional network of nanoparticles all bound to each other by DNA linkages and this will drastically couple the plasmons, resulting in a color change that is easily visible to the human eye. This requires that the target DNA concentration be higher than that of

the nanoparticles in order to achieve a reasonable color change. Given this requirement, there may be concern that this would not provide the kind of sensitivity needed to detect the low amounts of DNA that are important in so many clinical scenarios. Ultimately, the detection limit of this method depends on several factors including the size of the nanoparticle, the affinity of the probe to the analyte, and the degree of plasmon coupling upon binding, which is dependent on the inter-particle distance. Recall, however, that nanoparticles have an extremely high extinction coefficient, and as such can produce a visible color in solution at approximately nM concentrations [12], which would allow for DNA detection at a comparable magnitude.

If, however, the test needed to detect very dilute quantities of nucleic acids that are in the pM range or less, then it would need some way to enhance either the signal coming from the nanoparticle aggregation or the reaction causing nanoparticle aggregation. Many studies have focused on the former strategy, choosing to increase the intensity of the signal by using sensitive electrosensors or by attaching other reporter molecules to the nanoparticle like fluorophores or catalysts [22-24]. These efforts defeat the original benefit of nanoparticles, which is their innate color intensity and that their color change can be observed without laboratory equipment or extensive procedures. Instead, this study adopts the strategy of enhancing the reaction that causes aggregation. This was achieved by establishing recursive amplification of the basic analyte to nanoparticle binding event, which amplifies the effective concentration of the analyte.

The strategy of amplifying the effective analyte concentration is nothing new to the field of DNA detection. The most common amplification scheme for DNA is polymerase chain reaction (PCR) [5], but this technique requires a thermocycler and

sensitive polymerase enzyme, which again defeats the goal of simplicity. Instead, this study employs enzyme free-DNA reactions, most notably the hybridization chain reaction (HCR) developed by Dirks and Pierce [25]. By incorporating DNA strands capable of undergoing cascading hybridization reactions, multiple NP linkages can be formed from a single target DNA, which can, in turn, lower detection limits compared to conventional colorimetric detection schemes. The next section focuses on the operation of the DNA reaction networks that make this possible.

DNA Reaction Networks

There are many ways to exploit the complimentary hybridization of DNA beyond just storage of genetic information. One of the first, and intuitive, engineered application of DNA was for structural purposes. DNA can be used to create self-assembled, branched structures on the nanoscale including periodic arrays [26, 27]. Such systems are designed by synthesizing short single strands with specific binding domains to other strands. Linkages are formed spontaneously by complimentary hybridization. More tightly folded patterns can produce "DNA origami" of any shape, which is a technique considered for fabrication of nano-scale electronic or optical device scaffolds [28, 29]. For several years, the engineered applications of DNA remained static structures being formed from a pool of components and then resting in a final functional form, but further development yielded dynamic DNA reactions, most of which operate wholly or in part by a process known as toehold-mediated strand displacement [30].

Toehold-mediated strand displacement TMSD is a process whereby one DNA strand replaces another's position as the hybridized pair to a third basal strand. The two stands competing with another must share at least a portion of their sequences that is

complimentary to the base strand. If the two competing strands have roughly the same degree of thermodynamic complimentarity to the base strand, then either matching is equally favored, resulting in no particular hybridization preferences. This is often the case in genetic recombination events [31]. If, however, the invading strand is more complimentary, either by having a more correctly matching sequence or by simply being longer and having more complimentary bases than the initial strand, then the displacement reaction favors the invading strand (Fig 1.4). This can serve as a programmable driving force for rearranging hybridization partners and thus as a force for detectably changing the state of the system.

It should be noted that the TMSD process does not proceed by complete spontaneous disassociation of the initial duplex, leaving room for the new hybridization partner. Rather, the invading strand gradually replaces the previous partner base by base in a random branch migration process. The step time for each nucleotide exchange is on the order of milliseconds, so the rate of strand displacement reactions between oligonucleotides is usually more limited by diffusion and binding to the toehold than it is by branch migration rates [31, 32].

One of the earliest engineered applications of this principal was for clinically relevant DNA detection by Ellwood *et al.* in 1986 [33]. In this study, strand exchange was used to release a fluorescent marker into solution when the analyte strand displaces the marker. Up until this study, most sequence-dependent DNA detection methods, such as southern blotting, relied on binding a probe directly to the immobilized analyte, which is labor intensive, consumes a large amount of analyte DNA, and tends to produce background noise during the staining process [34]. By contrast, the method employed by

Elwood *et al*. used untreated soluble analyte to release an immobilized reporter strand and the resulting solution can be easily and sensitively tested for fluorescence. This early technique already possessed the feature of using DNA reactions to switch the chemo-physiological state of the system, but the significance of using DNA's dynamic reaction potential was not immediately realized. This early study presented their mechanism as merely a tricky, indirect form of probing for a DNA sequence.

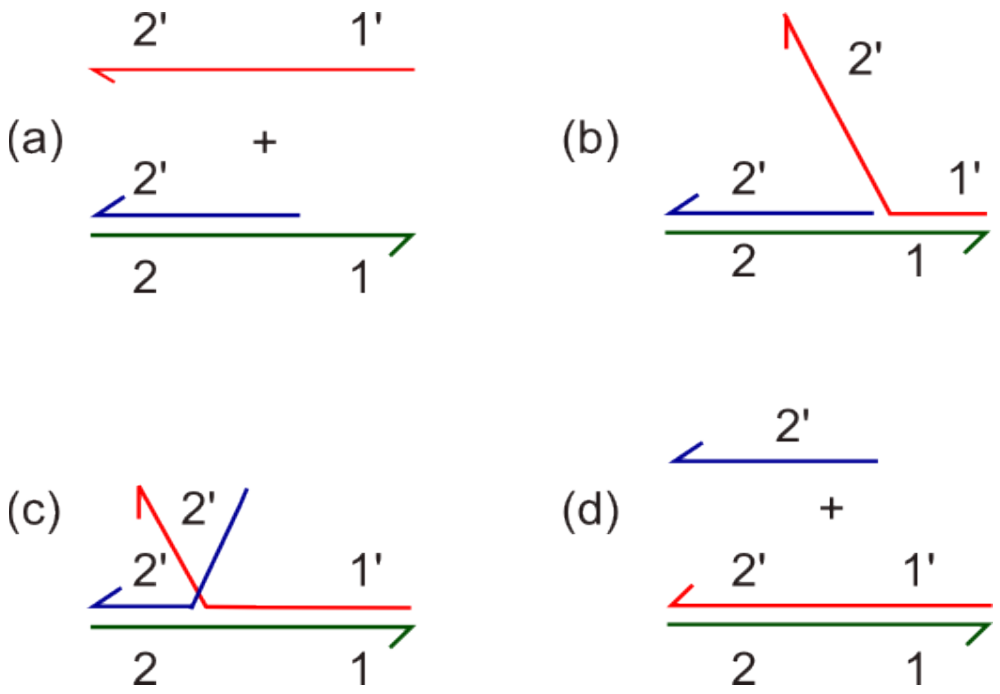

Figure 1.4 Toehold-Mediated Strand Displacement. a) The invading red strand contains a domain (1') that is complimentary to an unbound toehold on the green basal strand. b) The invading strand hybridizes to the toehold. c) The invading red strand and the blue strand compete for base pairing with the green basal strand. The process is random, and the zipping and unzipping does not have a biased direction in the middle, but because the invading strand has a toehold, it can never be fully removed. The blue strand, however, can fall off if the invading strand hybridizes completely to the base. d) The random walk is such a rapid process (much faster than the rate at which the invading strand finds the base strand) that it doesn't take long for the competition to reach, by chance, the state where the invading strand is fully hybridized in the contested domain. When this happens, the blue strand is released.

Eventually, biology offered more inspiration as more active forms of nucleic acids were discovered. Nucleic acids can act directly on compounds in the form of ribozymes [35], or they can interact with each other and regulate activity in the case of siRNAs and riboswitches [36, 37]. It became a regular analogy to describe cellular control mechanisms as little chemical circuits with feedback controls, and input/output logical components. With this mindset, it's not a far stretch to want to use those simple circuitry elements to build your own circuits for chemical reactions. There are several kinds of logic-performing DNA reaction networks [38-40] and even DNA machines capable of performing mechanical work [41-43], but this study focuses primarily on triggered DNA switches that produce an amplified response. We shall review three examples.

The first example switch will be the seesaw logic gate developed by Qian and Winfree [44]. This reaction operates entirely by reversible TMSD events and is driven by a net increase in entropy. The reaction starts with a base strand, output strand, and fuel strand hybridized in a non-equilibrium ratio. Both the output strand and the fuel strand can occupy the same hybridization position on the base strand, but the initial state of the system is such that the entire base strand is hybridized to output strand and the fuel strand is free floating. The fuel strand does not possess the appropriate toehold to displace the output strand and is thus kinetically blocked from achieving thermodynamic equilibrium (Figure 1.5). Equilibrium would occur if the output and fuel strands hybridized to a percentage of the base strand that is proportional to the molar ratio between output and fuel strand. The introduction of a small amount of catalyst strand allows for the base strand to exist as an intermediate that either the output or fuel strand can invade and this

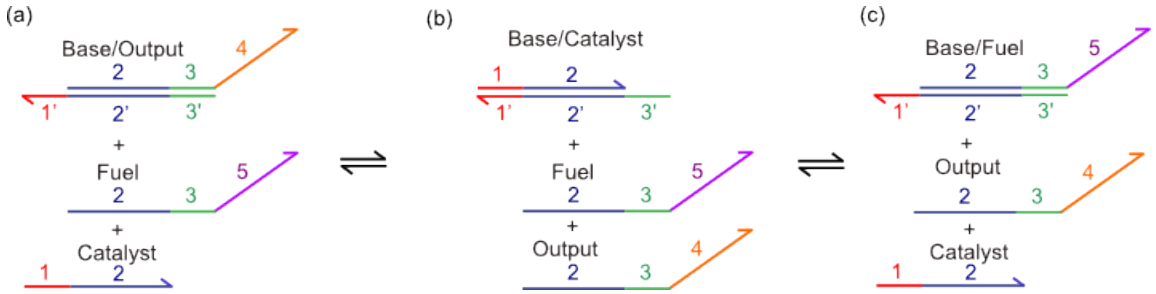

Figure 1.5 Seesaw Switch Mechanism. a) The base/output complex and the fuel strand are metastable in the absence of the catalyst strand. If the catalyst strand is added, it can bind to the base strand and perform TMSD. The toehold hybridizations are transitory and the 2 domain is needed for a more permanent hybridization. Catalyst can displace output strand, but there is no net gain in base pairing once the output strand dissociates, so this step is reversible. b) The removal of the output strand produces an intermediate base/catalyst complex, which has an open 3' toehold that either the fuel strand or output strand can bind to and perform TMSD. c) If the fuel strand invades the base/catalyst complex, it produces a base/fuel complex and regenerates the catalyst. All of these reactions are reversible, so the equilibrium state will have base/output, base/catalyst, and base/fuel in a ratio proportional to the molar ratio between output, catalyst, and fuel strands respectively. Having more fuel than output will favor the production of base/fuel from base/output provided that there is catalyst to form the requisite intermediate. The release of the output strand can then be measured with DNA detection techniques to quantify the amplified response.

allows the system to relax into thermodynamic equilibrium. The release of the output strand is then used as the signal that the reaction has proceeded (Figure 1.5).

Another catalytic switch was devised by Zhang *e. al.* that offers exponential signal output via an autocatalytic mechanism [45]. This design also features a base strand pre-hybridized to an output strand, as well as a fuel strand in solution. There are two primary differences between the Zhang *et al.* design and Qian and Winfree design. First, the fuel binds non-reversibly to the base strand. Secondly, the initial base strand complex contains the output strand and a releasable catalyst strand. A simplified autocatalytic design based on the Zhang *et al.* design is shown in Figure 1.6. The result is that each cycle of this mechanism releases the input catalyst strand and a second catalyst strand,

which increases the reaction rate as the reaction proceeds. Note also that the reaction is entropically driven by the fact that three species are consumed (the fuel, catalyst, and base/output/catalyst complex), yet four species are produced (output, two catalyst strands, and the base/fuel complex).

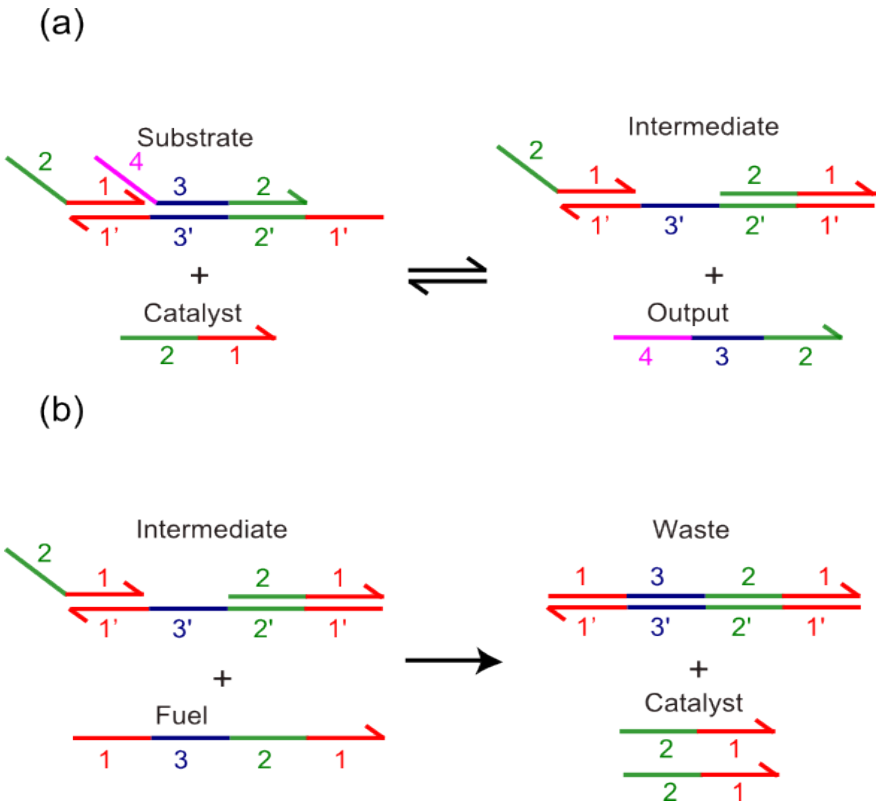

Figure 1.6 Autocatalytic Switch Mechanism. a) This switch is composed of a substrate complex containing a base strand, an output strand, and an inactive catalyst strand. The introduction of a free catalyst releases the output strand and produces an intermediate complex. b) There is also fuel strand in the reaction solution that can invade the intermediate and this invasion releases the two catalyst strands and produces a waste complex. The first step in the overall mechanism is reversible, but the second step is not and thus, the overall mechanism is non-reversible. The waste strand has no toeholds for invasion and the net reaction produces more strands than are consumed which is the entropic drive for this reaction. Since the overall mechanism regenerates the catalyst and releases a second catalyst, the reaction is autocatalytic, and the output can be released at an exponential rate.

The third switch we will examine is the most relevant to our study and, unlike the previous two, is driven by a gain in enthalpy rather than entropy, and this feature will prove useful when attempting to form aggregates of gold NPs. Hybridization Chain Reaction (HCR) is another catalytic switch that requires the addition of a catalyst strand to activate [25]. The HCR system is composed of two hairpin DNA strands, which are kinetically trapped in a metastable state. DNA hairpins are single strands that fold back and hybridize to themselves. The hairpins in this case assume the form shown in Figure 1.7 in that they have a single stranded toehold, a double stranded neck, and a single stranded loop that connects the backbones of the strand segments that are hybridized to each other in the neck region. The HCR system is locked in a metastable state, which means that there exists a lower energy, and thermodynamically preferred state where all the hairpins are hybridized into chains, but the system has a kinetic barrier.

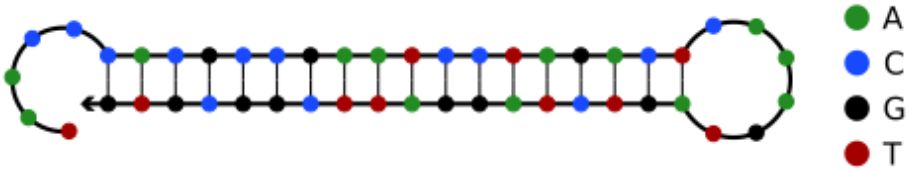

Figure 1.7 A DNA Hairpin. This structure is formed when a length of the DNA sequence is complimentary to a nearby sequence on the same strand. Because DNA has reverse complimentarity, the relative orientation of the two strands must be opposite, which is easily performed by a simple loop. The double-stranded region of self hybridization is often called the "neck" region, and the unpaired bases between them are referred to as the "loop" region. If the loop region is sufficiently short (around 6-10 bases), the nucleotides therein are not easily accessed by their compliments. Because of this latter trait, hairpin structures can effectively hide unbound domains with chemical potential to hybridize that cannot be accessed until the hairpin is opened somehow. The hairpin shown is a NUPACK rendering of one of the hairpins used in this study [46].

As the name suggests, the HCR system is designed to initiate a recursive hybridization of the metastable hairpins when triggered by the presence of catalytic amounts of the initiator strand. The process, illustrated in Figure 1.8, begins with a solution containing hairpin 1 and hairpin 2. If the initiator strand is added, it binds to the a toehold on hairpin 1 and this anchor mediates strand displacement of the b' domain from the hairpin, such that, the nucleotides that are paired with the b domain are replaced one by one with the equivalent nucleotides from the initiator strand. Next, the exposed c domain and the displaced b' domain act similarly to the initiator strand towards hairpin 2. The c domain binds to the c' on hairpin 2 and this toehold mediates another strand displacement, which opens up hairpin 2, exposing its loop and a b'. This exposed sequence is equivalent to the initiator strand, and therefore can bind to and unfold another hairpin 1 strand, thus ensuring the propagation of the cycle.

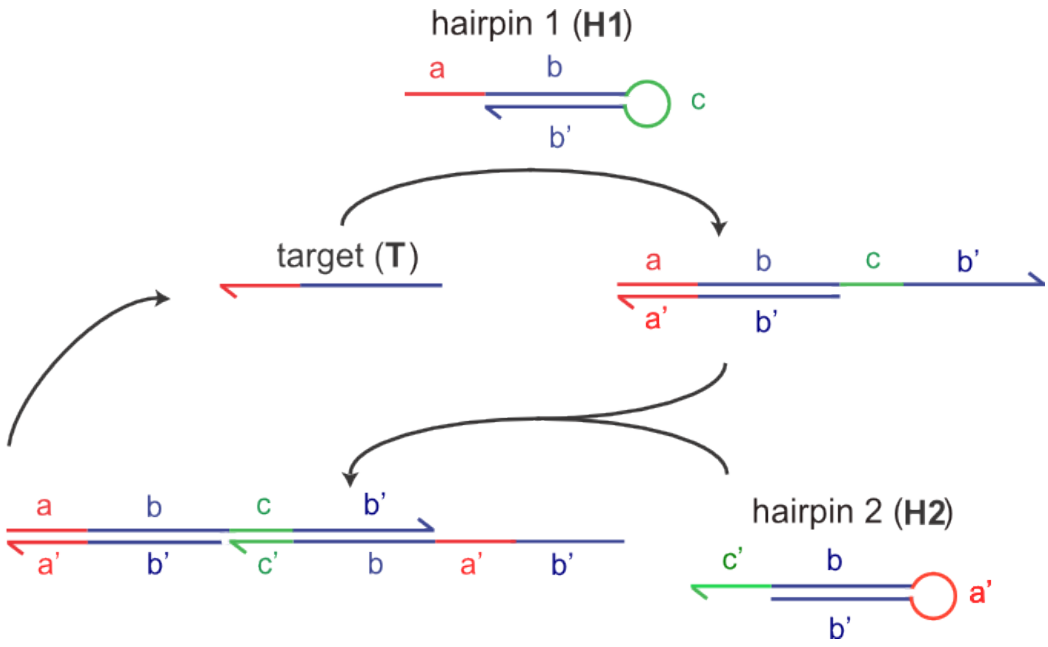

Figure 1.8 Mechanisms for Hybridization Chain Reaction. The target molecule first binds to the toehold on hairpin 1. This event unfolds hairpin 1 via toehold mediated strand displacement and exposes the c domain. The c domain binds to a

toehold on hairpin 2 and similarly unfolds that hairpin. When hairpin 2 is unfolded, it exposes a region that is identical in sequence to the target strand and can therefore start another start the cycle again by binding to another hairpin 1.

As an analogy to polymer chemistry, one can view the exposed toehold and b' region as an active center, which is consumed in each iteration of the cycle but creates a new active center in the next monomer on the growing polymer. The exposed toehold and b' domain behave in a similar fashion since they constitute a reactive state that gets transferred to each successive hairpin strand in the reaction and enables that strand to perform toehold-mediated strand displacement with the next hairpin strand. The reactive state does not exist in the initial test solution of two hairpins because the hairpins start out in a closed form. The reactive state is introduced in the form of the target strand, which is open and has the exposed toehold and b' domain. Once introduced, the reactive state can be recursively transferred to the leading end of the polymer of hairpins. Compared to free radical polymerizations, however, HCR does not suffer from a termination analogous to the combination of two radicals, since two b' sequences cannot hybridize.

Even without fluorophores or other readout strategies, the initiation and propagation of HCR can be analyzed by gel electrophoresis. As shown in Figure 1.9, the hairpins are stable when mixed together but without any initiator added. When the two hairpins are mixed together, they maintain a state where each hairpin is un-reacted and there is only one size of DNA element present. Once the initiator is added, larger products become evident in the gel as higher bands, and they are produced by chain reaction. The lengths of these DNA multi-mers are inversely proportional to the amount of initiator used, since lower concentrations would cause less initiation sites and relatively more hairpins that could be added per initiation site.

HCR, therefore, does not explicitly need gold nanoparticles in order to be applied for DNA detection, but the technique of gel electrophoresis, while being a fairly simple laboratory technique, is not exactly field deployable. Gold nanoparticles provide a simple readout alternative because a pre-made test solution could be combined with a collected sample, and positive detection could be seen visually as a color change.

Merging Two Methods

The research described in this study is an attempt to utilize two developing technologies in order to fulfill a real technological need. Cheap and easy-to-use DNA sensors would allow easier screening for early cancer detection and could be used in remote locations or poor communities to fight disease epidemics. Gold nanoparticles offer a simple-to-use colorimetric test for a wide variety of analytes, but the detection limit can only go so low while still keeping the test simple and not requiring many enhancement steps or advanced instrumentation. DNA-based amplification reactions, however, allow for a small amount of DNA to cascade into a large amount of output DNA to detect. The goal is to couple such a cascading DNA reaction to nanoparticle aggregation such that very low concentrations of a target DNA sequence of interest can elicit a strong optical change in the test solution that is visible to the naked eye. In the three subsequent chapters, we demonstrate how several modified DNA reaction networks were applied to create gold NPs capable of catalytic aggregation.

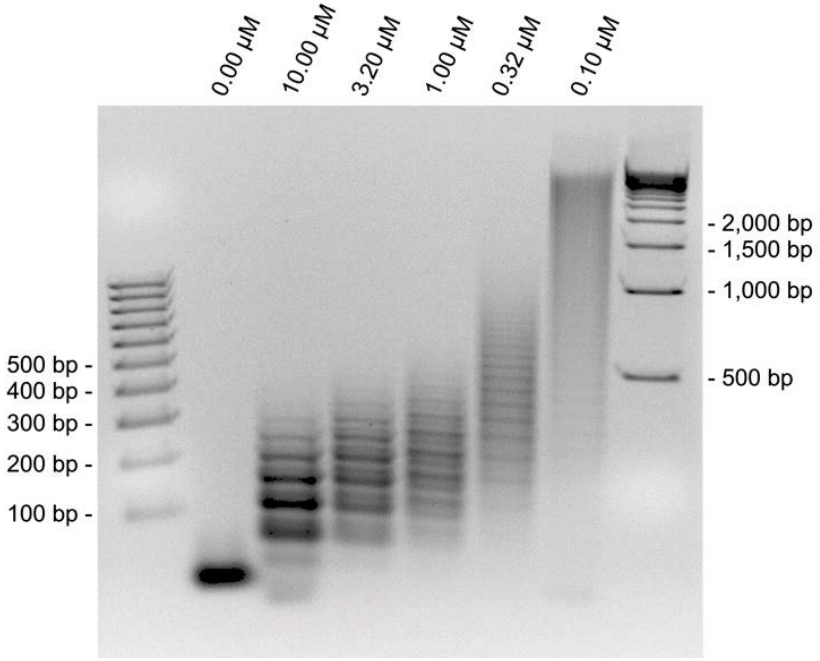

Figure 1.9 Gel Electrophoresis Analysis of Hybridization Chain Reaction Products. The flanking lanes contain DNA ladders. Each of the inner lanes shows the reaction product of a solution containing 1 µM of each hairpin strand as well as a concentration of initiator strand shown above each lane. Without any initiator strands added, the hairpins (each the same size) remain intact and un-reacted. Note that sub-stoichiometric quantities of initiator consume all of the hairpin strands, confirming that the reaction reiterates. Also note that lower concentrations of initiator form larger products since all of the hairpins are used up, but from fewer nucleation sites. Image from Dirks and Pierce [25]

CHAPTER TWO: DESIGNING, TESTING, AND ANALYZING CASCADING AGGREGATION NETWORKS

General Approach

Since our goal is to trigger many nanoparticles into aggregating using a small amount of DNA initiator, we chose a DNA amplification network that starts with many isolated strands but collapses into a state with significantly more multi-strand complexes. There are many DNA reaction networks to choose from, but for our first attempt at a catalytic aggregation of gold nanoparticles, we selected Hybridization Chain Reaction (HCR) devised by Dirks and Pierce for its simplicity, stability, and for its formation of long polymers of the DNA reactants [25].

To realize colorimetric HCR tests, we decided to simply attach gold nanoparticles to each of the hairpins, such that polymerization of hairpins would polymerize nanoparticles into a network that could theoretically accomplish plasmon coupling and result in a color change. To make this strategy work, several design modification had to be made. Each modification was motivated by the performance of the previous design. The subsequent sections in this chapter review those experimental efforts.

Attachment Procedure

All of these NP aggregation schemes depend on having DNA probes attached to the nanoparticle surface, so the first step in executing each design is the production of functional NPs. The most common means of attaching DNA to metallic gold is to use

thiol-modified synthetic DNA strands [47]. The sulfur in the synthetic DNA's thiol group covalently bonds to gold. Thiolated DNA was purchased from IDT Technologies and gold nanoparticles were synthesized using the sodium citrate method [48]. In brief, a 0.25 mM solution of chloroauric acid was brought to a boil 1 mL of 0.51 mM sodium citrate solution was added and boiling was continued for 10 minutes. The resulting gold colloid was characterized by UV-vis spectrophotometry on a Cary 100 Bio scanning in the wavelength range of 700-400 nm. The size and concentration of the gold nanoparticles was calculated from the absorbance peak and using extinction coefficients and absorbance peaks for nanoparticles of various sizes found in previous studies [21].

The thiolated DNA strands came with a 6-mecaptohexanol protecting group to be cleaved with a reducing agent prior to incubating with gold nanoparticles. For this we used a 100 mM solution of freshly prepared dithiothreitol (DTT), which was incubated with the DNA for 1 hour. Excess DTT and the protecting alkane thiol were removed by running the DNA solution through a NAP-10 desalting column. The eluate was tested for DNA content using the same spectrophotometer, scanning in the range of 350-200 nm. The DNA concentration was calculated using the strand’s estimated extinction coefficient at 260 nm. Next we took the reduced DNA and mixed it in a 500 to 1 ratio with the gold nanoparticles solution. This solution was then buffered to 10 mM phosphate (pH = 7.4) and 0.01%, by mass, sodium dodecyl sulfate (SDS).

After a 24 hour incubation, in which the thiols are attaching to the nanoparticles surface, the salt concentration was raised to 0.3 M using four subsequent additions of 4 M NaCl with additions spaced 30 minutes apart and added drop-wise with stirring. The salted solution was then left for another 24 hours. This salting process helps to drive the

functionalization further by increasing the ionic strength of the solution and decreasing the repulsion between DNA strands [49, 50].

With the salting complete, the particles were then purified three times by centrifugation to remove excess DNA strands. This was done by spinning the solution at 10,000 rpm for 30 min, removing the clear supernatant, and re-suspending the pelletized NPs in fresh buffer. The particles concentration was again measured by spectrophotometry, and the particles were then ready for aggregation experiments.

Design One: Conventional Nanoparticle Control

In order to qualify the performance of catalytic aggregation systems, there needs to be a point of reference. For this purpose, a conventional design was used as a performance standard. The conventional design consists of two nanoparticles with probes complimentary to different halves of the target strand to which they bind and form a single bridge much like in the study by Elghanian (Figure 2.1 a).

For visual simplicity, Figure 2.1 only shows one DNA strand attached to each nanoparticle. A design with just one probe strand per nanoparticle would work if such particles were stable, but you may recall that spherical gold nanoparticles often need many DNA strands in order to infer enough hydrophilicity for the nanoparticles to be stable in solutions of biologically relevant ionic strength. It is difficult to control the exact number of DNA strands attached to the surface of each nanoparticle, but it is often desirable to maximize the DNA load per particle and thus to use an excess of DNA, which can be purified away from the nanoparticles later. It is estimated that gold nanoparticles can be loaded with 180 +/- 20 DNA thiolated strands per 20 nm

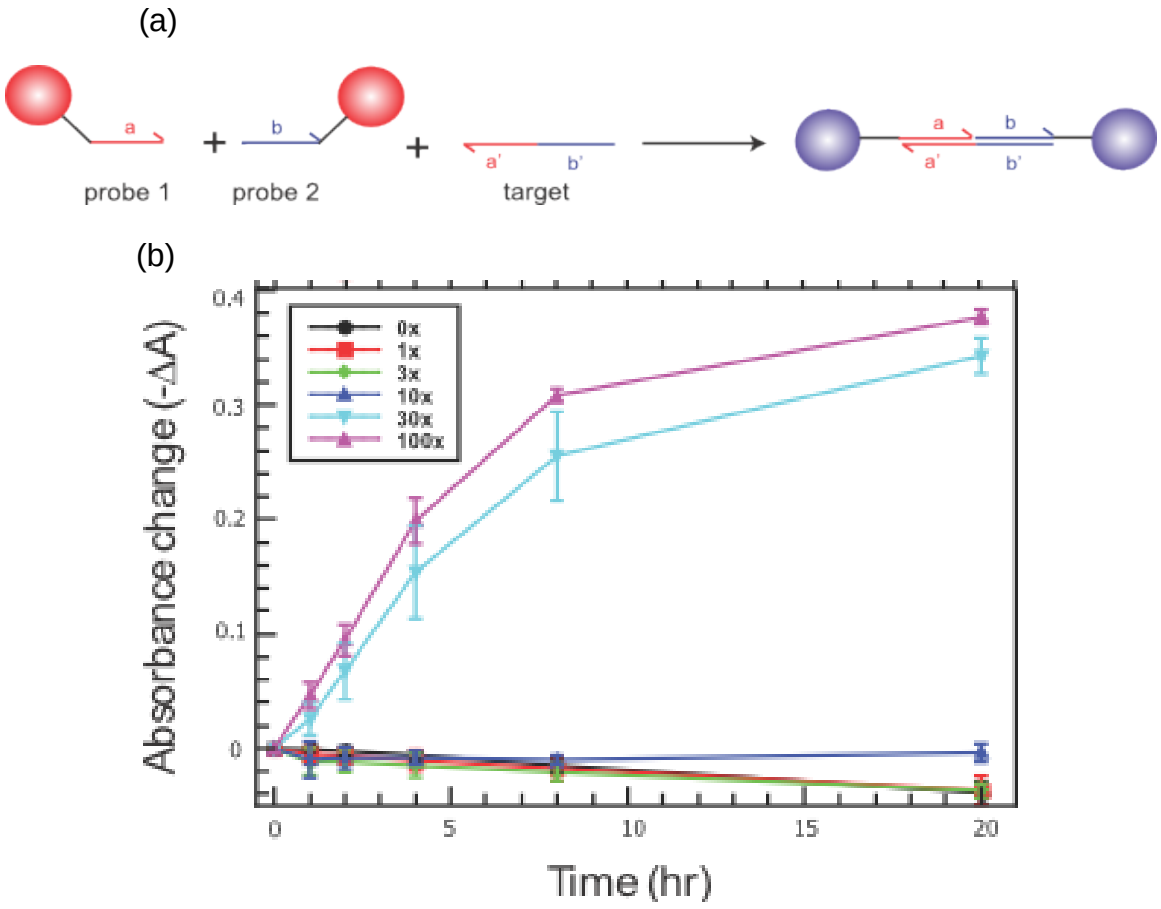

Figure 2.1 Direct Aggregation. a) Two nanoparticle types were used in this assay, each coated with a different DNA probe. The two probes bind to different halves of the target strand through complimentary hybridization. Binding of both NPs to the same target molecule results in a coupling event and thus a color change. b) The absorbance data collected over time. Each data set is a separate reaction. Each reaction contains 1.57 pM of each nanoparticle and the listed multiple of that concentration of target strand. Aggregation is measured as a drop in absorbance (-ΔA). There is a discrete detection limit, where notable aggregation requires that the target concentration be 30 times that of the nanoparticles for good multivalent networking. Some of the reactions triggered with low target concentrations exhibit slightly negative values for –ΔA, potentially due to nanoparticles settling to the bottom of the cuvette, where the detection laser is aimed.

particle [51]. We used an excessive ratio of 500 strands per particles to ensure maximum DNA loading. The exact DNA sequences used for each strand are available in Table A.1 in the appendix.

A test solution containing the two NPs was subjected to varying concentrations of the target strand to determine a detection limit. The extent of aggregation can be qualitatively observed with the naked eye, but quantitative study required the use of a spectrophotometer. The test solutions were scanned in a Cary 100 Bio spectrophotometer in the visible spectrum (400-700 nm) both before the introduction of target strand and after an incubation time of 24 hours. The color change manifests in the spectrum as a peak shift, a peak intensity drop and a general broadening of the absorbance peak. The results obtained with this first design can be seen in Figure 2.1 b. Absorbance drop and peak shift were both measured, but only the absorbance drop data is shown because the peak shift values are more variable and become difficult to measure at high degrees of aggregation. The target strand concentrations are listed as multiples of the nanoparticle concentration (157 pM). In order to induce significant aggregation, the target must be present in a concentration that is 30 times that of the nanoparticles. In evaluating the subsequent designs, we used that target/NP ratio (30x) as the detection limit of a direct aggregation design. Also note that aggregation in this design plateaus at about 0.4 A.U. of absorbance drop and it generates up to about 40 nm of peak shift for the 30x and 100x (not shown).

Design Two: Two Hairpins

Our First approach to merge the simple colorimetric readout of gold nanoparticles to the already functioning amplification network of HCR was to simply attach nanoparticles to each hairpin strand. As the hairpins hybridize into long polymers of alternating hairpins, the nanoparticles would then theoretically also be arranged into linear arrays, but with cross links. Since each nanoparticle has multiple hairpins of one

type on its surface, then each nanoparticle can also act as a bridge between separately nucleated polymers of hairpins, ideally resulting in a branched and tangled aggregation of nanoparticles and DNA.

Making the hairpins attachable to gold nanoparticles required two modifications. The first modification is the addition of several thymine residues on the 5' end of hairpin 1 strand or to the 3' end of hairpin 2 as shown in Figure 2.2. This poly-T region serves as a spacer (sp), which ensures that the toeholds of the hairpins are physically separated enough from the nanoparticles surface such that the nanoparticle does not block the approach of the incoming target strand, which must hybridize to the toehold. In a study by Park *et al.*, it was found that a spacer region of 12 thymines was sufficient to prevent the nanoparticles from creating steric hindrance for the hybridization reaction of their nanoparticles [52]. By comparison, our design has bulkier DNA probes because of the secondary structure of the hairpins, but we chose to keep the number of thymines in the spacer at twelve for the sake of coupling distance. We cannot simply make the spacer region arbitrarily large to avoid steric hindrance because the end goal is to link the nanoparticles with certain proximity for plasmonic coupling. The second important modification to the HCR design was adding a thiol group to the toehold end of each hairpin (on the terminal thymine of the spacer region), which allows the strand to chemically bond to the gold surface. The sequences are available in Table A.1 in the appendix. Note that the signal strand used in this design is a different sequence than that used in the direct aggregation design.

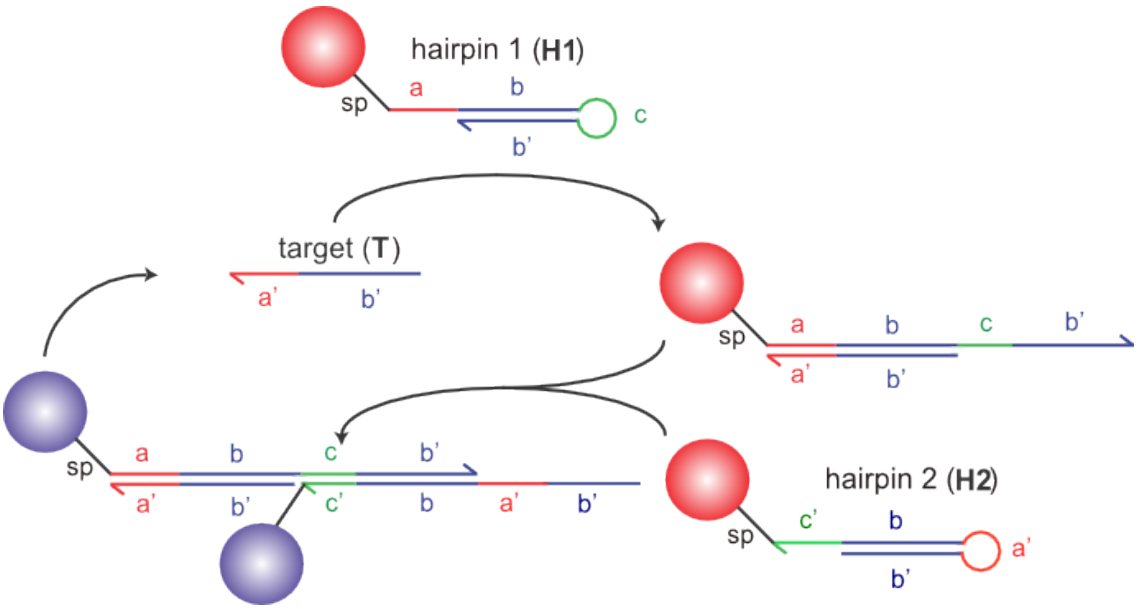

Figure 2.2 Mechanism of HCR on Nanoparticles. Free target molecule binds to the toehold on hairpin 1, which unfolds the hairpin, allowing its loop domain to bind to a toehold on hairpin 2, which also unfolds. The two nanoparticles are now linked and they have a free tail with the target sequence, which can start another cycle by interacting with another hairpin 1.

There is a wide range of gold nanoparticle sizes with a peak absorbance in the visual range, but the selection of the proper size depends on several factors. For efficient plasmonic coupling, the inter-particle distance should be approximately equal to, or less than, the nanoparticle diameter [53]. Once incorporated into the growing HCR polymer of hairpins, the distance between two adjacent nanoparticles would be about 21.6 nm, assuming the strands were relatively straightened and the spacer regions angled away from the polymer. This estimation was calculated by the number of nucleotides between the nanoparticles (72) and an estimated average length contribution of 0.34 nm per nucleotide[54]. Thus, the particles should be at least 20 nm in diameter to match this length. The nanoparticles cannot be made arbitrarily larger than this value because we also have to consider solubility. If the particle is too large, but the DNA length stays

fixed, the DNA will not be able to provide enough negative charge to keep the gold particles suspended in salty solutions. Thus we selected nanoparticles of 25 nm in diameter (the same size that was used in the direct aggregation experiment), which we synthesized in our lab using the sodium citrate reduction method described previously.

The functional nanoparticles were produced and a series of aggregation experiments similar to those performed for the direct design, were used to estimate a detection limit. Early attempts showed no signs of any aggregation, and the procedure was modified heavily from that used for the direct aggregation scheme in order to induce aggregation. Due to the modifications used, only the peak shift was measured for this design, not the absorbance drop. The most important modification was the increase in the salt content of the buffer, which was doubled from 0.3M NaCl to 0.6 M. With this modification, the NPs could aggregate at target concentrations as low as five times that of the NPs (Figure 2.3). By comparison, the catalytic design (design 2) is more sensitive than the conventional design (design 1) if you consider the detection limit alone, but not by the magnitude expected for such a radically different mechanism. This catalytic design also did produce as much peak shift when it did aggregate (only about 7 nm of shift rather than 40 nm observed in design 1). The comparison is slightly invalidated by the differences in the target concentrations used as well as the difference in reaction buffer.

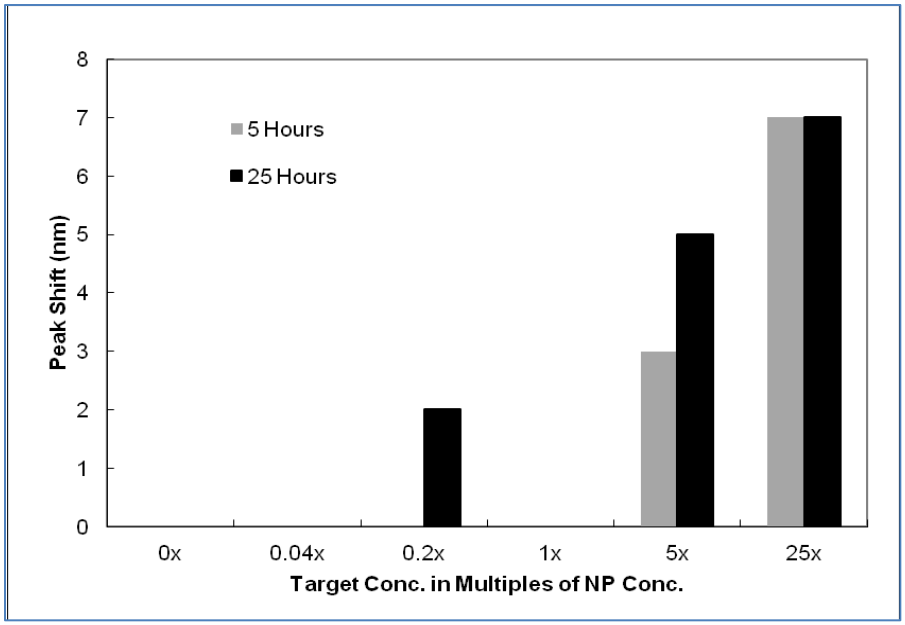

Figure 2.3 Two Hairpin Design Aggregation. Peak shift was measured as increase in peak absorbance wavelength relative to the peak absorbance of the negative control at 0 hours of reaction. The 5x and 25x reactions were considered to have notable aggregation. The 0.2x reaction did not appear to have changed color significantly and the measured peak shift may be an outlier caused by either a scanning error or contamination with the target.

The fact that design 2 required more salt did, however, provide clues to help troubleshoot the design's limited performance. DNA strands naturally repel each other due to their negative charge. Cations from the buffer help to partially neutralize this charge so that the DNA strands do not repel each other and this process is known as the screening effect [50]. The fact that increased screening helps this reaction proceed implies that it is limited by DNA crowding or even nanoparticle crowding.

The problem lies within the binding of the DNA hairpins to nanoparticles. Compared to the classical HCR mechanism, where individual hairpins float freely in solution, the hairpins in this design are tightly packed onto nanoparticles. This change hinders the reaction in three ways. First, the strands that are bound to the nanoparticles

are not in the ideal orientation for hybridization because their toeholds are closer to the nanoparticle than the neck and loop regions are. Secondly, the hairpins experience more DNA repulsion as they approach a dense field of hairpins than they would approaching a single hairpin. Finally, and most importantly, the catalytic design must contend with steric hindrance between NPs. The first two NPs that bind together are no more crowded than in the case of direct aggregation, but the third NP must wedge itself between the previous two in order for DNA strands on its surface to hybridize with the growing HCR polymer (Figure 2.4). This was not an issue with the direct aggregation design (design 2) because each new DNA bridge between NPs forms separately and can therefore form where other NPs are not in the way. Our next design sought to partially overcome these crowding effects.

Design Three: Linker/Target Complex

The previous design had issues with DNA crowding that could only be overcome with high salt content. Ideally, the test system operates in buffers of biologically relevant pH and ionic strength so that adding the sample does not interfere with the test reaction. This third design was created with two goals in mind: to fix the crowding issues such that the test can be performed under the same conditions as the direct aggregations design, and to fix the crowding issues so that the test would be even more sensitive.

Our approach was to separate the inter-particle bridges from each other, such that they were connected by discrete divalent attachments rather than arrayed on a long chain of hairpins, while retaining the ability of HCR to propagate after each bridge formation. Thus, one of the two hairpins, rather than exposing an attached active region, must

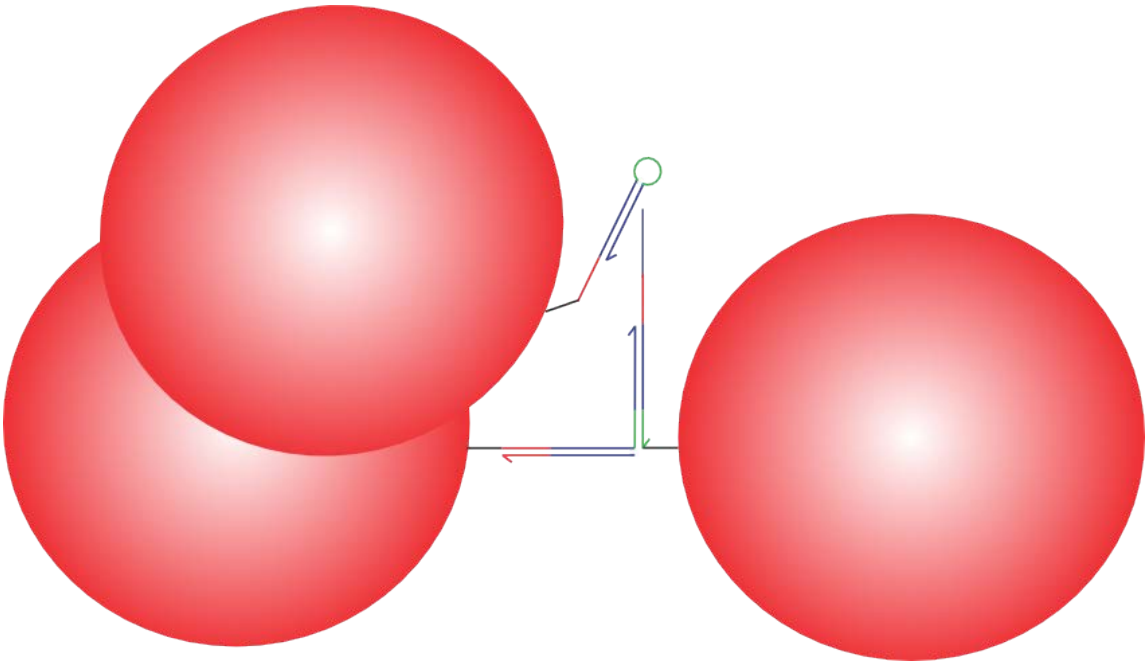

Figure 2.4 Steric Hindrance Between Nanoparticles. In the catalytic aggregation design (design 2), only two nanoparticles can easily attack to each other per target strand present. The DNA bridge between the nanoparticles has an exposed active sequence that could theoretically bind to a third nanoparticle, but because the DNA strands uses are shorter than the nanoparticle diameter, it is difficult for a third nanoparticle to fit in the inter-particle gap and approach the active sequence at the proper orientation. This flaw in the design doesn't prevent the system from aggregating with sufficient concentrations of the target strand, but it offers no sensitivity advantage over the conventional direct aggregation because it can still only bind two nanoparticles per target strand.

release an active element to trigger the next cycle. This can be achieved by the mechanism shown in Figure 2.5 a. The primary modification here is that hairpin 2 has been cleaved between the b and a' domains. The segment that contains domains c' and b is still capable of fusing to the opened hairpin and will thus serve as a bridging element to the second nanoparticle. This strand is no longer a hairpin and has been renamed "linker." The other strand, which contains domains a' and b', will be released, and since it is identical to the target sequence, it can trigger another hairpin strand to open elsewhere. This fragment is appropriately renamed "target" strand.

Note that the linker strand now has a different orientation with respect to its covalently attached nanoparticle. Whereas hairpin 2 had the spacer and thiol modification on the 3' end of the b domain, the linker strand extends a spacer region from its 5' end. This allows for even more inter-particle distance and allows the particles to bind to each other in the more preferred "tail to tail" fashion [25]. Repositioning the nanoparticle was not necessary for the linker/target adaptation, but was done to help alleviate steric hindrance and is allowed now that there is no longer a loop domain at the 3' end of the b domain.

These design modifications were expected to increase catalytic potential and therefore to increase sensitivity to the target. Once again, the detection limit was evaluated by subjecting the combined nanoparticles to varied concentrations of the target strand and measuring an absorbance drop, just as design 1 was tested. When thus tested, however, this design was too unstable; to the extent of being self-triggering (Fig. 2.5 b). The negative control solution, which contained nanoparticles with hairpin 1 and linker/target, respectively, underwent significant aggregation without the introduction of additional target strand. The phrasing "additional target strand" is now necessary since the test solution contains the linker/target complex. One might reasonably ask if there is any excess or residual target strand left over from the production of the nanoparticles coded with linker/target complex.

In troubleshooting this design, we first attempted to increase the stringency of the purification step. In our functionalization process, once the attachment of DNA to the

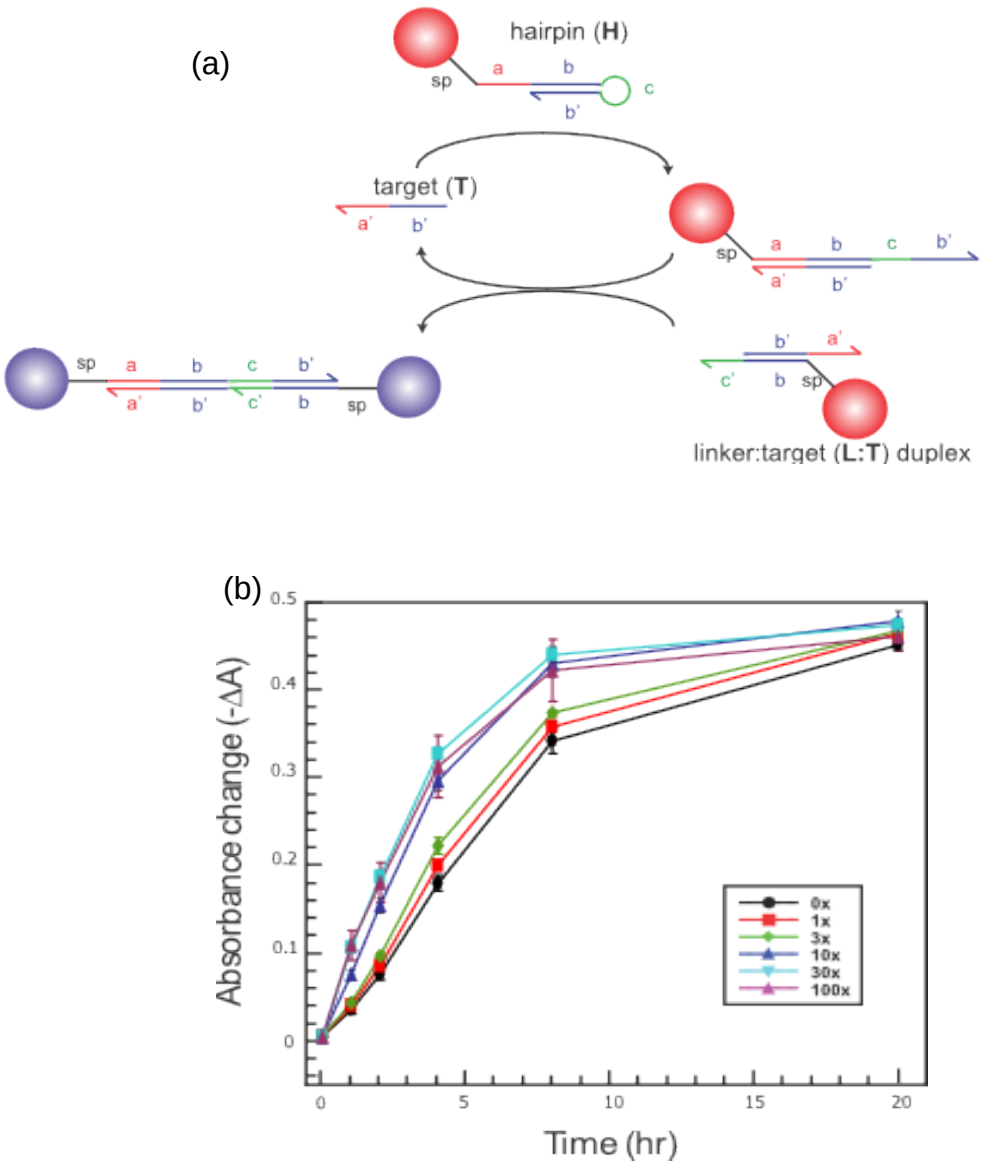

Figure 2.5 Catalytic Linker Design. a) The test solution in this case contains one nanoparticle type with hairpins attached and one with a linker/target complex attached. The target strand thus already exists in the solution, but is sequestered and not able to initiate the reaction. Reaction mechanism starts when the target strand invades the hairpin. The opened loop domain invades the linker/target complex and displaces the previously sequestered target molecule, which can start the cycle over again. b) The aggregation results of this design exhibit severe instability. Even the negative control (0x target) aggregates rapidly, most likely due to the supposedly sequestered target strand from the linker/target complex.

nanoparticle is completed, excess strands are removed by centrifugation. During each spin, the heavy nanoparticles collect at the bottom of the tube, but unattached DNA

strands remain in solution. After the spin, the majority of the supernatant is removed by pipette with special care not to disturb the viscous, liquid pellet of nanoparticles. This necessitates that a small portion of the supernatant not be removed and thus the purification is not 100% effective. The exact residual volume for each iteration of this purification varied, but was often around 5% or less of the total solution that was centrifuged. Thus we can expect that every repetition of the spinning, removal and re-suspension should effectively remove 95% of the excess DNA strands. By default, each batch of nanoparticles undergoes 3 repetitions of the purification process and should thus achieve a 99.9875% removal of excess strands. Increasing the number of spin cycles to 6 was still not sufficient to prevent self-activation and it is unlikely that further purification would prevent it.

Another possibility for the self-activation is that the linker/target complex, even if present in a perfect 1/1 ratio, can disassociate post-purification, thus releasing the target strand trigger into solution. This is also unlikely based on the thermodynamics of this hybridization. DINAMelt hybridization simulation software estimates the free energy of this complex to be 33.6 kJ/mol, which would make for a disassociation constant on the order of 10^{-25} [55]. As such, spontaneous disassociation is probably not the culprit.

The most likely mechanism for self-triggering is a strand exchange between a linker/target complex and a hairpin 1 mediated by the a domain. Note from Figure 2.5a that the red a domain on linker/target complex is available for hybridization to the a' domain on the hairpin. Strand exchange was prevented in the original HCR design by

concealing the toehold in inaccessible loop regions of the hairpins. By effectively cleaving hairpin 2 at its loop region, we inadvertently allowed access to the a' domain. Our next design focuses on remedying this error.

Design Four: Linker/Target with Protecting Group

Our goal with this design was to make the a' domain on the linker/target complex less accessible to hairpin 1 in the un-reacted state, yet still completely accessible once released from the linker strand by an activated hairpin 1. Our strategy was to hybridize part of the a' domain to the linker strand. Specifically, three of the thymines on the 3' end of the b domain were replaced with residues complimentary to a' domain across from them, thus extending the double-stranded region of the linker/target complex. The 3 nucleotides that replaced the thymines are here collectively referred to as the protecting group. The modified linker/target complex is shown in Figure 2.6 a.

This approach has advantages and disadvantages. On one hand, it leaves fewer nucleotides available to be used as a toehold for the premature strand exchange mechanism, but on the other hand, it hampers the reaction with the target. During the second stage of our aggregation mechanism, the opened hairpin 1 binds to the linker strand via the c domain and proceeds to displace the b' domain of the linker strand. In our previous design, this severs all base pairing between the linker and the target, but in this design, the linker strand is still held by 3 bases. A three-base toehold is far from permanent, but it is possible that the random walk of branch migration might proceed in the other direction before this disassociation happens. Recall from Chapter 1 that the driving force for toehold-mediated strand displacement is correlated to the enthalpic difference between the before and after states. Whereas the previous design had a net

(a)

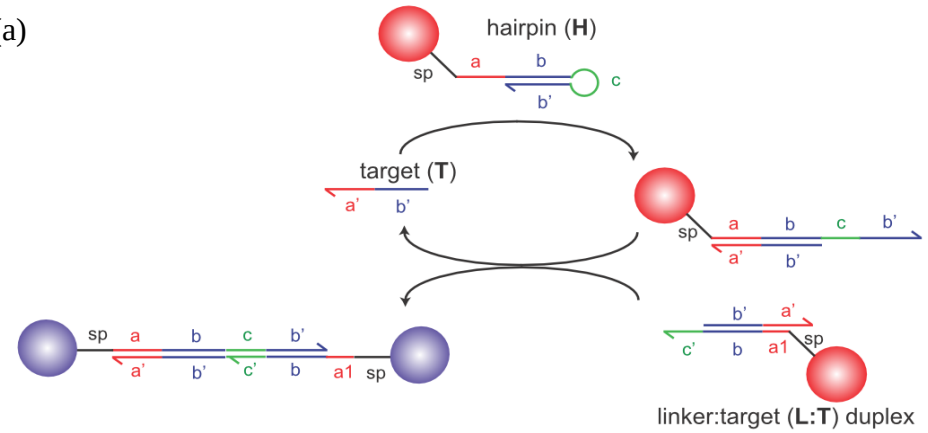

(b)

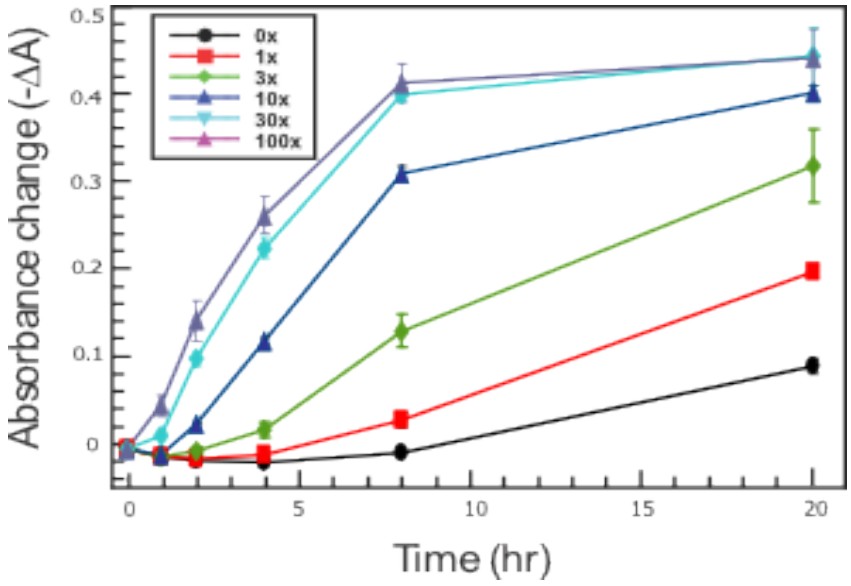

Figure 2.6 Protected Linker Design. a) The mechanism is the same as the linker/target design except for the inclusion of an a1 domain on the linker strand, which is only half the length of the a domain. This protecting domain keeps the target strand in the complex from having a full toehold to prematurely interact with hairpin strands. b) The protecting group drastically improved stability. There is still aggregation occurring in the negative control (0x) but it is mild compared to the reactions with moderate levels of target strand added.

gain of 6 base pairs (from the toehold), this modified design has a net gain of only 3 base pairs (gains 6 from the c domain but loses 3 from the protecting group). It may be somewhat misleading to consider these toeholds in terms of such concrete numbers of

nucleotides. In reality, double-stranded DNA has a certain degree of “breathing” at the ends where the complimentary nucleotides spend some time unhybridized [56]. Because of this, the reduced toehold effectively has more than just three nucleotides for initial binding. We could cover the toehold completely and reduce the false positive reaction considerably, but this would hinder our favorable HCR reaction, so we chose to protect only half of the toehold as a safe middle ground.

Figure 2.6 b shows the aggregation results using various concentrations of the target strand initiator. Given enough time, the negative control still aggregated and eventually produced a false positive, but the degree of aggregation in the negative control was decreased by incorporating the protecting group. The reactions triggered with high concentrations of the target produced an absorbance drop of about 0.4 A.U. and 40 nm of peak shift (similar to the high concentrations in design 1) but the negative control showed roughly a fourth of that absobance drop and even less peak shift. In fact, the reactions triggered with only 3x or 10x target (target to nanoparticle ratio) induced significant absorbance drop beyond the leakage and can be considered a positive result for the test. This is an improvement over the conventional direct aggregation design that required at least 30x target to aggregate. Thus, this design could still be used as a colorimetric test provided that the two nanoparticles are mixed just prior to adding the analyte and that the measurements are taken before the background color change proceeds too far. Practical application of this design would also require a negative control be run with every test, such that one can tell if the test reaction has proceeded significantly faster than the un-triggered control reaction. So, while there is a workaround for the false positive reaction, it involves an extra step.

Another consequence of the leakage is that it imposes a barrier to lowering the detection limit of our colorimetric test. In the absence of any background aggregation, an arbitrarily small amount of target strand could aggregate every nanoparticle in the solution if given enough time. In this case, there would be theoretically no detection limit, only a question of how long of a time scale is considered acceptable. With the leakage, however, the analyte concentration must be high enough to produce color change that is detectibly faster than the rate of leakage. One way to improve the detection limit therefore would be to increase the rate of the desired reaction (open hairpin 1 displacing target on the linker/target complex) relative to the leakage reaction (target strand reacting with hairpin 1 while still attached to linker).

Note that we could theoretically decrease the leakage rate even further by expanding the protecting group on the linker to include more complimentary bases to the a' domain on the target strand. However, this will also decrease the rate of hairpin 1 displacing the target strand. But as mentioned before, if we made the protecting group hybridize to all 6 bases of a', there would be no thermodynamic advantage for hairpin to displace target. A protecting group of three bases successfully reduced the false positive reaction relative to the activated reaction, but there is still opportunity to try different lengths of protecting group to optimize the reaction rate ratio. Before devoting any more resources to that optimization, our next design priority was to address a more pressing question.

Design Five: Shortening the Bridge

When comparing the conventional design (design 1) to the protected linker/target design (design 4), the cascading DNA reaction has increased sensitivity (showing notable

color change as low as 3x target rather than requiring 30x target) but we must be careful drawing conclusions from this comparison. Many of the experimental variables were made equivalent when testing these two designs, such as nanoparticle size, nanoparticle concentrations and target DNA concentrations, but there are several factors either out of our control (with the given procedure) or overlooked that prevent us from definitively declaring an improvement.

First, the average number of DNA strands per particle was not measured for any of the nanoparticles produced. We used what was considered to be an access of DNA for the given surface area of gold based on other studies [27] but the maximum loading may vary in our different designs. The catalytic designs use hairpins or complexes on the nanoparticle surface whereas the conventional strand has linear single-stranded DNA that should theoretically pack more efficiently. A difference in nanoparticle loading would change the effective concentration of reactive DNA elements given the same nanoparticle concentration, which could affect the reaction rates we are trying to compare.

Secondly, the target sequences are not the same for the conventional design and the catalytic designs. Ultimately, the goal of this research is to use these designs to detect clinically relevant nucleotides sequences, such as part of a viral genome or a microRNA whose up-regulation might indicate cancer. For now, this study focuses only on proof of concept and used sequences from HCR for the catalytic designs. Ideally, these general designs need only be engineered down to the domain level, and the particular sequences can be altered depending on our "target" sequence of interest, but sequence changes are not necessarily going to be thermodynamically equivalent. Replacing a G-C pair in the toehold with an A-T pair for instance would decrease the rate of toehold binding. When

comparing the reaction rates between different detection designs, the target sequence would ideally be the same, but they are not (See Table A.1 in the appendix).

Lastly, the designs cannot be directly compared because the inter-particle distance is not the same. Thus far, the degree of aggregation has been measured indirectly as an absorbance drop, but optical shifts from plasmon coupling are proximity dependent, so the differences in absorbance drop could be attributed to either more linkages being formed or by the particles being closer.

For a better comparison, the next nanoparticle aggregation design uses a shortened version (nucleotides removed from the sequence) of design 4 (our best catalytic design at that time) to more closely match the spacing in the conventional designs. The spacer regions were reduced by 8 thymines and the b domain in all relevant strands was shortened by the deletion of 6 nucleotides from the center of the domain. The lengths of the inter-particle bridges are shown in Table 2.1. The new design is coined short linker/target and is, on the domain level, equivalent to the protected linker/target design shown in Figure 2.6 a. Sequence differences (Table A.1).

Table 2.1 Inter-particle Spacing

Design	Bridge Length in Nucleotides	Estimated Bridge Length in nm
Design 1	48	16
Design 3	72	24
Design 4	75	25
Design 5	51	17

It was expected that bringing the particles closer would increase the optical response given the same aggregation rate, but comparing the data from the last design to this shortened version (Figure 2.6 b and Figure 2.7, respectively), we see relatively similar absorbance drop rates for the higher target concentrations although it should be noted that the peak shift was roughly twice as high at every concentration for design 5 than design 4, which indicates that shortening the bridge has a higher impact on peak shift than it does on absorbance drop. Furthermore, at lower concentrations, the short design performs worse than the previous design in that it required a full 24 hours before the 3x is distinguishable from the leaking negative control. These lower reaction rates

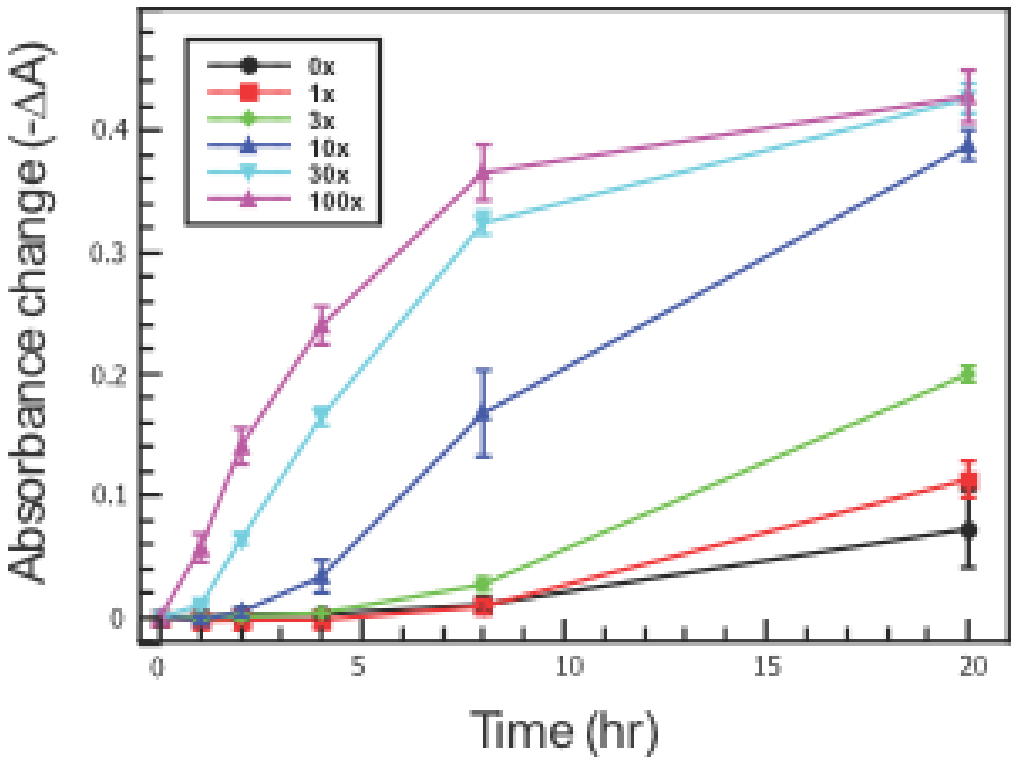

Figure 2.7 Short Linker Results. The aggregation results for this design are similar to that of the protected linker/target design, with the exception that the reaction seems to proceed slower in the lower concentrations of target strand. There is still background aggregation when the two nanoparticles are mixed, but concentrations as low as 3x can be reasonably resolved from this background level.

may be due to steric issues around the nanoparticle now that our toeholds are closer to the nanoparticle surface and therefore are theoretically more crowded by their neighboring. strands. The reaction rate may also have been lowered by the closing of the inter-particle distance causing more particle crowding. Despite these limitations, the shortened design is a better comparison to the direct aggregation design, and the lower detection limit observed in the shortened catalytic design supports the claim that nanoparticle-based colorimetric detection can be made more sensitive by incorporating DNA amplification networks, even under spatial engineering constraints. These designs could be further optimized to decrease the rate of the false positive and to increase the rate of the triggered reaction. The next section is concerned with the principals used for optimization, and potential changes to the designs.

Maintaining Metastability

The primary challenge with any DNA-based amplification system is establishing the appropriate level of metastability. There must be a sufficient thermodynamic advantage to the end state in order to drive the reaction forward, but there must also be sufficient kinetic traps to prevent the transformation into the final state prior to adding the catalyst strand. In the preceding designs, such enthalpic drive was supplied by the formation of more base pairing between the toeholds and loop domains of the system.

For example, in the original HCR mechanism, proposed by Dirks and Pierce, each toehold binding event results in six more bases being bound to their compliment releasing an estimated 1-3 kJ/mole. This enthalpic gain outweighs the entropic loss of reducing the total number of DNA complexes. The subsequent nucleotide displacements along the neck region are considered to be enthalpically neutral since there is no net gain in the

degree of base pairing. Rather, some of the nucleotides of the hairpin are being replaced with those from the target strand. Each step in the mechanism is therefore driven by the toehold hybridization.

The process is thermodynamically spontaneous, but is held in check by the limited availability of the toehold's compliment on the other strand, which is physically blocked by nature of being in the loop region of the hairpin. This kinetic barrier is sufficient to prevent reaction between the hairpins provided that certain conditions are met. As the length of the loop domain increases, the single-stranded DNA becomes less crowded and strained and more closely resembles a dangling single-stranded end. Increasing the length of the loop region allows for the spontaneous reaction between hairpins and the rate of this spontaneous reaction increases with the size of the loop [57, 58]. For this reason, the loop domain used in the adopted form of HCR and all derivative designs was kept to the optimal length of 6 nucleotides, which literature suggests is not too short to cause excessive physical strain, but is not too long to allow hybridization with the loop region until it is opened [57].

However, design 3 necessitated the opening of the loop region of hairpin two by cleaving the DNA at the 5' end of the a domain. Compare Figure 2.2 and Figure 2.5. The linear form of this dangling end is expected to be the primary culprit of the false positive observed in this design's aggregation experiment. The supposed mechanism of this false positive starts with the binding of the a' domain on the linker/target complex to the a domain on hairpin 1. The strand displacement reaction that follows is unconventional in that it involves four strands rather than three. It is unknown whether each four-strand exchange would be more sterically hindered than a simple three-strand exchange since it

is anticipated that the three-strand exchange would involve invasion via the major groove of B-DNA, which would not permit enough room for an entire double-helix [59]. The four-strand exchange mechanism may therefore require a certain degree of spontaneous strand dissociation, perhaps assisted by the physical strain incurred by binding the toehold in an unfavorable orientation, in order to proceed. With this anchor, the system then relaxes to a lower energy state by exchanging the b' domain of the hairpin for the b' domain of the target on the hairpin. In light of this predicted interaction, the design challenge was then to reduce the availability of the a' domain on the linker/target complex by some other means.

Design 4 accomplished this by partial sequestration of that a' domain. This was done by the addition of three nucleotides between the linker sequence and the spacer region (the 15 thymines on the 5' end), which are complimentary to the a' domain. This modification has the advantage of slowing the false-positive mechanism, but decreases the enthalpic advantage of the intended reaction since the net gain of base pairing has decreased from 12 to 9 base pairs now that 3 more pairs must be broken. The aggregation experiments suggest that the sacrifice is well worth it. Compared to design 3, design 4 exhibited substantially less aggregation in the un-triggered reaction, yet is still capable of detecting the DNA target strand with reasonable peak shift. This success illustrates the importance of understanding how the availability of the toeholds and the thermodynamic drive influence the reaction's kinetics, and ultimately, the assay's performance. Along with maintaining metastability, the other critical consideration for these designs has been the consequences of localizing these DNA reaction networks to a nanoparticle surface

and how to avoid steric hindrance. These same principles proved useful for subsequent projects discussed in the following chapters.

CHAPTER THREE: APTAMER TRANSDUCERS

Expanding the Candidates for Analytes

The previous sections have only addressed using nanoparticle-based assays to detect a nucleic acid target. However, the principal of using gold nanoparticle aggregation and a DNA reaction network for signal amplification would be valid for a wide variety of analytes as long as there is a way for the analyte to trigger nanoparticle aggregation. The following experiments describe how an aptamer was used to make adenosine a trigger for the nanoparticle-based amplification network.

Aptamers are single-stranded nucleic acids whose sequence is capable of binding to a particular molecule through a complex folding of hydrogen and Van der Waals bonds [60-63]. This behavior is more akin to protein folding and binding sites than the traditional Watson-Crick base pairing regularly associated with DNA. As such, the exact configuration of binding is difficult to predict, and logically engineering an aptamer sequence for a given analyte is currently prohibitively difficult. Aptamers are instead screened by affinity selection and enrichment from a random pool of sequences. This process is known amongst molecular biologists as SELEX (Systematic Evolution of Ligands by Exponential Enrichment) [64].

As an example, an aptamer for adenosine triphosphate (ATP) was developed by Huizenga and Szotak from a pool of 10^{14} random oligonucleotides, each flanked by the same primer sequence for later amplification [65]. The pool itself was created by

synthesizing a given sequence imperfectly. The primer ends were synthesized normally, but each nucleotide to be added to the internal region used a cocktail of nucleotide triphosphates as the reagents, allowing for a controllable “mutation” rate.

This pool of oligonucleotides was run through an ATP-linked agarose column such that those strands capable of binding to ATP stalled longer in the gel. The selected nucleotides were then eluted and amplified by PCR. This selection process was repeated several times. The aptamers created in this study also have a high binding coefficient to ATP derivatives, such as ADP, AMP, and even adenosine. This study is heavily cited and the aptamer sequences have been used in assays for ATP and adenosine for biological applications or simply as a model system for aptamers in general [1, 18, 61, 63, 66].

Such aptamers have already been employed in conjunction with gold nanoparticles to create colorimetric assays for non-nucleic biomolecules [67-69]. However, none of the designs in these previous studies include any means of inherent amplification and therefore can couple, at most, two nanoparticles per aptamer binding event. Furthermore, aptamers have previously been used to trigger catalytic DNA networks, including HCR [25]. Specifically, Dirks and Pierce produced an aptamer construct that undergoes conformational change when binding to the analyte. This conformational change exposes a region with the HCR initiating sequence (Fig. 3.1). This method used aptamers to trigger HCR, but used high concentrations and gel electrophoresis to detect HCR. To our knowledge, ours is the first attempt at using aptamers to trigger an amplification network coupled to nanoparticle-based colorimetric readout.

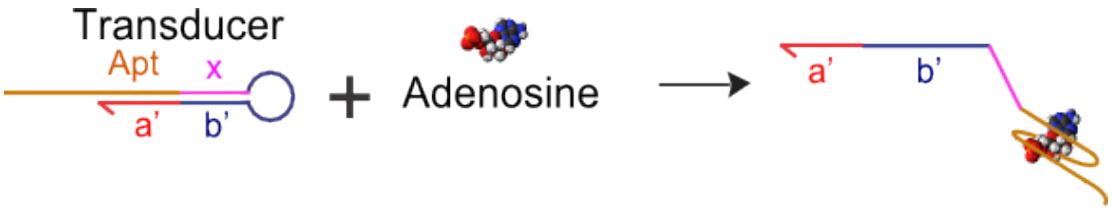

Figure 3.1 Aptamer Transducer. The transducer is composed of a hairpin structure and a dangling toehold. It contains an aptamer sequence that takes up the entirety of the tail and part of the neck region. When ATP, or adenosine, starts binding to the aptamer tail, the rest of the aptamer unfolds from the neck to envelop the ATP. This leaves the neck region weak enough to unfold entirely, which exposes the triggering sequence for HCR.

Design Adjustments

Our basic strategy was to use a transducer hairpin similar to Dirk and Pierce's construct in order to initiate our protected linker/target design (design 4 from Chapter 2). Again, the transducer element contains both an aptamer to adenosine and a sequence for triggering the amplification. The transducer is the only element in this system that contains an aptamer sequence. Previously, we referred to the triggering DNA sequence as the target strand because it was the nucleotide sequence our test was designed to detect, but here our ultimate detection target is adenosine, so we will rename the target strand to signal strand for applications with aptamer. Because the sequence for the aptamer portion of the transducer is determined by the affinity selection and is also partially complimentary to the initiator sequence, our sequence limitations prevent us from using our previous linker/target amplification design without changing the sequences.

Keep in mind that the amplification network can be triggered in two ways. We may either introduce the initiator strand, or we can add a combination of the transducer and adenosine. Adenosine will bind to the aptamer domain and competitively displace the portion of the initiator domain that is hybridized to the aptamer. We are careful here not to use the term "toehold-mediated strand displacement" because this is not one nucleotide

displacing another in a zipper-like fashion. Here we have a small biomolecule with non-Watson-Crick interactions replacing the Watson-Crick pairing in the transducer's neck domain. The exact mechanism of this displacement is speculative, but if it is successful, as the study by Dirk and Pierce suggests, it will expose the initiator strand and thus allow adenosine to indirectly trigger the amplification and the subsequent NP aggregation. Having two ways to trigger the reaction allows us to troubleshoot the design more easily by determining whether the amplification network is flawed or the transducer. The overall mechanism for our design is shown in Figure 3.2.

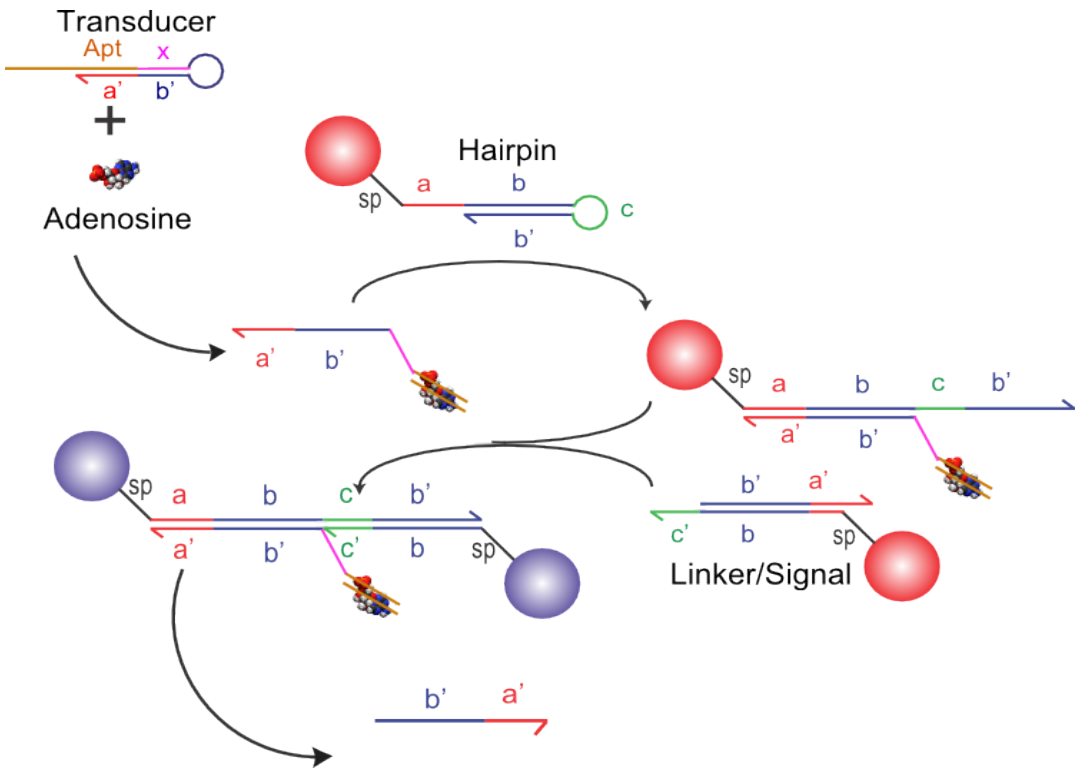

Figure 3.2 Aptamer-Based Mechanism. This design uses NPs with Hairpin and Linker/Signal complexes in much the same way as those shown previously. The difference is that it can be initiated by either the signal strand similar to previous designs, or by an activated transducer as shown. The transducer opens when adenosine binds to the aptamer portion and exposes the signal sequence. The transducer stays with the NP bridge, and a signal strand is released to initiate the next cycle.

Gel Tests

We decided to try out the new sequences with just the free DNA and no nanoparticles using gel electrophoresis to confirm proper operation of the DNA-level design. The various DNA strands were mixed in several combinations at 1 μM each in reaction buffer (0.3 M NaCL, 10 mM phosphate pH 7.4, 0.1% by mass SDS) and allowed to hybridize for 24 hours (complexes were first annealed at 95°C and cooled for 1 hour). A 3% Agarose gel was made using SB buffer (10 mM NaOH adjusted to a pH of 8.5 using boric acid) and an ethidium bromide concentration of 0.5 μg per mL. After the DNA hybridizations were complete, the samples were mixed with a glycerol and bromophenol blue loading dye and loaded into gel. The gel was run in SB buffer at 150 V for 25 min.

The hybridization of various components of the detection system is shown in Figure 3.3. The probe mixture of hairpin strand and linker/signal complex is relatively stable over four hours (lane 2) although some un-triggered hybridization did occur. The hybridization of the probe strands is easily initiated by the DNA signal strand, leaving no trace of the un-hybridized hairpin or linker/signal complex (lane 3). The transducer in closed form does not induce hybridization of the probe complexes (lane 4). The combination of 20 mM adenosine and transducer strand can induce hybridization, however (lane 5). When triggered by transducer and adenosine, the hybridization yields products of two sizes. The larger product is presumed to be a complex of hairpin, linker, and transducer strands while the smaller product is a complex of hairpin, linker, and signal strands. The smaller product is produced in higher numbers than when un-triggered. This suggests that the transducer/adenosine initiation not only starts

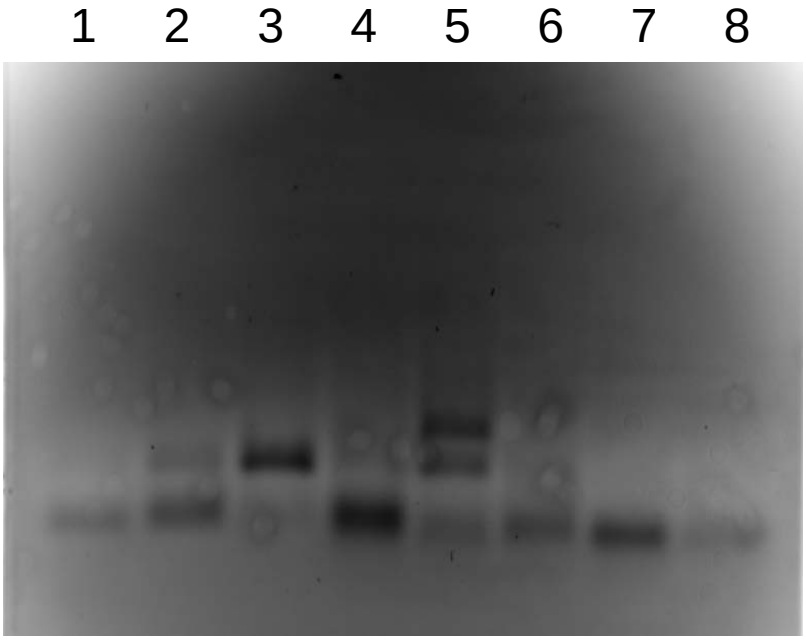

Lane 1:H
Lane 2: H + L/S
Lane 3: H + L/S + S
Lane 4: H + L/S + Trn
Lane 5: H + L/S + Trn + Ade
Lane 6: H + Trn + Ade
Lane 7: Trn + Ade
Lane 8: Trn

All DNA concentrations 1 μM
Adenosine concentration 5 mM

Figure 3.3 Combinatorial DNA Hybridizations. Each lane contains some combination of the DNA strands hairpin (H), linker/signal (L/S), signal (S), transducer (Trn), and the biomolecule adenosine (Ade). The first three lanes show that the amplification system works as intended when activated by a DNA initiator: the signal strand. Lane 2 serves as a negative control (the un-activated reaction) and Lane 3 represents the positive control (the reaction is activated by the signal strand). Lane 2 shows some evidence of self-triggering in that there appears to be a feint product band matching that of the activated reaction (Lane 3). Lane 4 represents the test system for adenosine, which is stable. Once adenosine is added to the full test system, the reaction proceeds and produces complexes of two sizes. The smaller complex is the H/L/S just as in lane 3, but the larger product is H/L/Trn/Ade, with Trn/Ade taking the place of the S strand. Lanes 6 through 8 are controls to monitor various other possible interactions and smaller steps in the overall mechanism. Note from lane 7 and lane 8 that there are no new bands to indicate the opening of the transducer's secondary structure. It could be that the binding coefficient is too low to notice, but still enough to trigger HCR, or it could simply be that the electrophoresis buffer and voltage disturbs the transducer/adenosine interaction or that the interaction is transient, allowing the electrophoresis process to separate them. This disturbance would not prevent HCR in the reaction for lane 5 since the components had 24 hours to react prior to being run through the gel.

hybridization between hairpin and linker/target, but is capable of releasing the signal strand for initiating the next cycle of hybridization. To ensure that the larger product was

not simply a multimer of transducer strands, a control was included with hairpin, transducer, and adenosine, which would not be able to form the complete complex of hairpin, transducer, linker, and signal (lane 6).

Aggregation

As before, one NP type was coated with hairpin 1 and the other type was coated with a linker/signal complex. Reactions were triggered with varied concentrations and combinations of signal, transducer, and adenosine. The added complexity of this system required the use of more controls. A negative control was used that contains both types of functionalized nanoparticles but was not triggered by either the signal strand or the transducer. A positive control for the amplification network portion consisted of the nanoparticles and a 30x concentration of the signal strand. Another negative control was performed using the nanoparticles and the transducer in the absence of adenosine. The remaining reactions tested the detection limit of the system for adenosine with a fixed transducer concentration of 3μM.

For this preliminary experiment, only the peak shift was measured for each reaction, not the absorbance drop. The aptamer sequence was inactive in the absence of adenosine (Figure 3.4), but produced aggregation when mixed with sufficiently high concentrations of adenosine. Two positive controls were tested. Both positive controls contained the nanoparticles and were triggered with 30x signal strand. The difference between the positive controls was that only one contained the transducer strand (without adenosine). Interestingly, the presence of the transducer inhibited the normal operation of the amplification module (Figure 3.4). We tested the opened and closed transducer strand

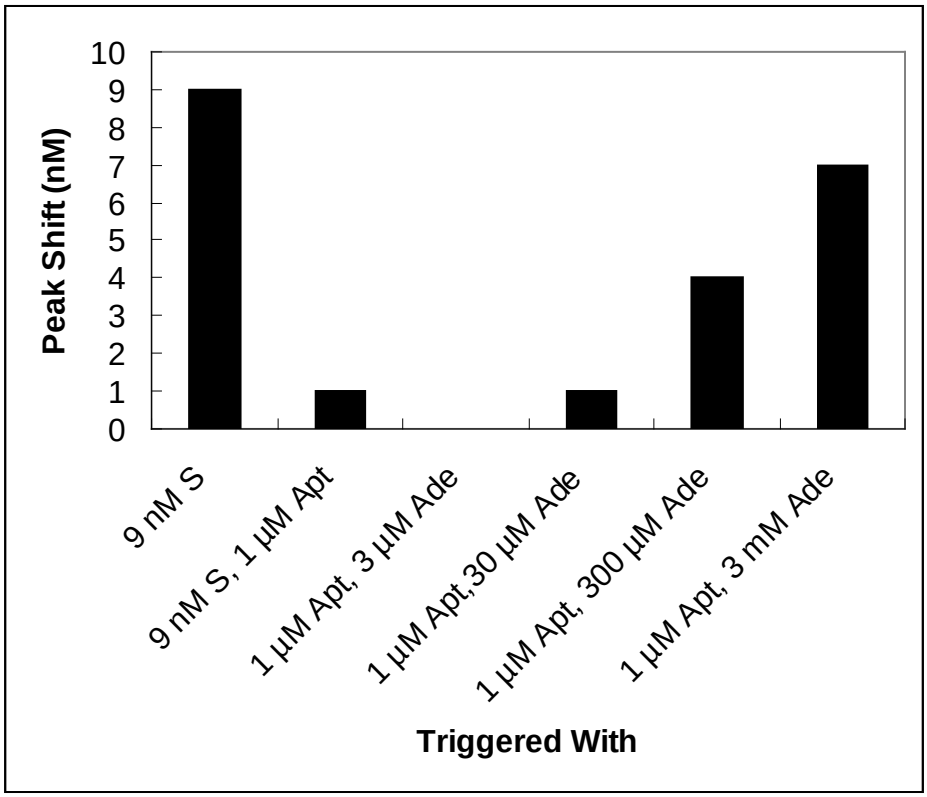

Figure 3.4 Aggregation Results for the Aptamer Detection Design. In each reaction, the two NP concentrations were fixed at 157 pM each, and aggregation was initiated with the listed reagents. This design requires high concentrations of adenosine to trigger aggregation when compared to using the triggering sequence. This may be related to inhibition of the catalytic cycle by the transducer strand. Note that signal-induced aggregation is inhibited by the presence of the transducer.

in NUPACK simulations in an effort to find the mechanism of inhibition, but none of the simulations predicted the transducer to bind with anything other than with hairpin 1 after being opened, as is intended.

Compared to the NP's detection limit for the signal strand (sub-µM range), the detection limit for adenosine is about 30 µM. This decreased sensitivity may be due to a poor binding coefficient of the transducer to the adenosine, as mentioned in the gel discussions above, but there is now evidence of perhaps a different culprit. If the transducer inhibits the positive control, which consists of the amplification module only,

then the amplification module should also be inhibited in all of the reactions with adenosine. More combinatorial DNA hybridizations were performed with gel electrophoresis to try to discover any unintentional hybridization possibilities. The hairpin strand did not hybridize to any of the strands it was not designed to, but when the linker was tested, it was found to hybridize to the transducer (Figure 3.4) even though the complimentary domains of the two strands (the b an b' domains) shouldn't be able to bind when the transducer's b' domain is concealed in a loop. The loop in this case is 10 nucleotides in length, which is potentially large enough to allow loop invasion [57]. This unintentional binding possibility is troubling, but it is difficult to imagine how it could be inhibiting the reaction since the same gel shows that the signal strand (which should be pre-hybridized to the linker) should prevents this interaction (Figure 3.4, Lane 4). The exact mechanism of inhibition is still unclear. It is difficult to devise design modifications to address the inhibition without knowing the mechanism, but design constraints are most flexible concerning the x domain of the transducer. As such, our next troubleshooting approach will be to adjust the thermodynamics of the transducer hairpin secondary structure by lengthening and shortening the x domain and thus adjust how much of the b domain is in the loop and how much is in the neck. This approach can help us fine tune the ease at which the hairpin opens in response to adenosine and its availability for interacting with the linker strand.

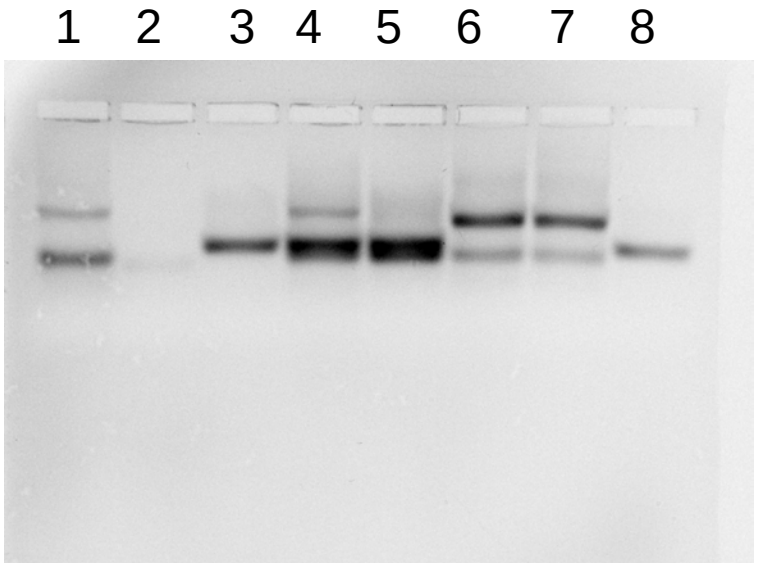

Figure 3.4 Possible Inhibition Mechanism. Each lane contains some combination of the DNA strands Linker (H), signal (S), and transducer (Trn). The "/" indicates species that were thermally annealed to each other. This gel was performed in an effort to discover unintentional hybridizations between the DNA strands in the network. When linker, signal, and transducer were present (Lanes 4 and 5) they exhibited bands that are merely superimposed combinations of the transducer and the linker/signal complex bands. These products were expected. When the linker and transducer were combined in the absence of the signal strand (Lanes 6 and 7), they created a higher band indicating hybridization between linker and transducer. This interaction was not intended.

These optimization experiments are pending, but we have at least proved that the approach of combining an amplification module and an aptamer transducer is valid and can result in detectible responses for the nanoparticle-based colorimetric test.

CHAPTER FOUR: AN ALTERNATE AMPLIFICATION SCHEME

Catalytic Hairpin Assembly

Many of the difficulties with self-activation seen in Chapter 2 hinge on the presence of the unpurified or self-released catalytic sequence in the test solution. While further modifications to the design or preparation of the nanoparticles might minimize self-activation, the only way to fundamentally solve this problem is to alter the underlying catalytic DNA network such that it does not contain the entire target sequence in the test solution.

An alternate DNA network for nucleotide detection is Catalytic Hairpin Assembly (CHA) designed by Li *et al.* [70]. This design also uses two metastable hairpin strands that hybridize together when exposed to a target strand. The primary difference between HCR and CHA is that the second hairpin unfolds towards the existing complex between the first hairpin and the target and actually displaces the target strand, resulting in a hybridization of the two hairpins while releasing the initial target strand (Fig. 4.1). In the original study, the opened hairpin 1 triggers a fluorescence increase, but the fused hairpins can also be used as linkers for gold nanoparticles, just as in the case of HCR. By releasing the same target strand that was used to hybridize the two hairpins, there is no need to incorporate the full catalytic sequence anywhere in the two hairpins or the test solution of nanoparticles.

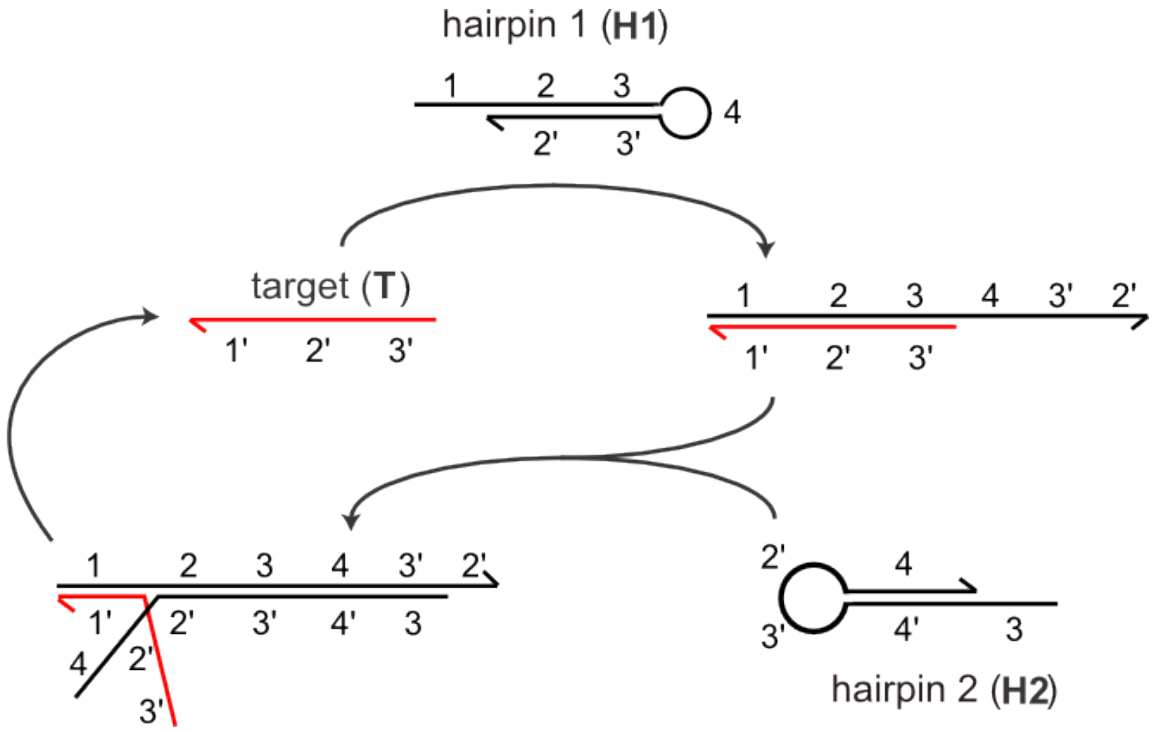

Figure 4.1 CHA Mechanism. Catalytic Hairpin Assembly reaction contains a mixture of two hairpins that will dimerize in the presence of a target sequence. The target first binds to Hairpin 1 and undergoes toehold mediated strand displacement to open the hairpin. The exposed region of Hairpin 1 then invades Hairpin 2, which opens and is in the correct orientation to unfurl towards the target, which it competes with and eventually displaces. The target strand is then free to start the cycle again with two more hairpins.

This alteration does come at a cost, however, since the second hairpin does not fully displace the target strand. The hairpin contains the necessary sequences to displace the 3 and 2 domains but not the 1 domain. Because of this, the target strand remains attached by eight nucleotides to the hairpin duplex. The 1 domain must therefore spontaneously disassociate in order to be released and trigger two other hairpins to hybridize. As another challenge, the released hairpin then has the opportunity to interact with either an un-hybridized hairpin 1 strand and thus form another nanoparticle bridge, or to interact with an already formed bridge again. Thus, the already hybridized hairpin duplexes serve as a sort of competitive inhibitor for the target strand.

Despite these limitations, CHA is still capable of maintaining metastability and relaxing it with the use of the target strand. In the original study by Li *et al.* on CHA, the activated hairpins exposed a reporter sequence to interact with a fluorescent dye-quencher pair and they tracked fluorescence as a metric for the extent of CHA reaction. The two hairpins were stable for up to 5 hours in the absence of target strand as evident in the lack of fluorescence increase associated with the opening of hairpin 1. Target concentrations as low as one hundredth that of hairpin 1 were sufficient to elicit significant fluorescence increase. In principle, this same sensitivity and stability can be converted into a colorimetric test, which does not require a fluorometer.

Design One: Attaching Nanoparticles to the Hairpins

Our first modification of CHA is illustrated in Figure 4.2. In short, gold nanoparticles and the requisite spacer region are added to the 5' end of each hairpin and the 5 and 6 domains were removed from hairpin 1 since they are no longer needed to interact with any dye-quencher pair. The modified sequences for the hairpins were used with nanoparticles in colorimetric aggregation tests as well as without nanoparticles in gel electorphoresis tests. The gel experiments were performed to confirm that the omission of the fluorescent reporter domains and the addition of the spacer have no significant effect on the CHA reaction. Figure 4.3 shows that the target strand is still capable of completely hybridizing the modified hairpins even when at sub-stoichiometric amounts.

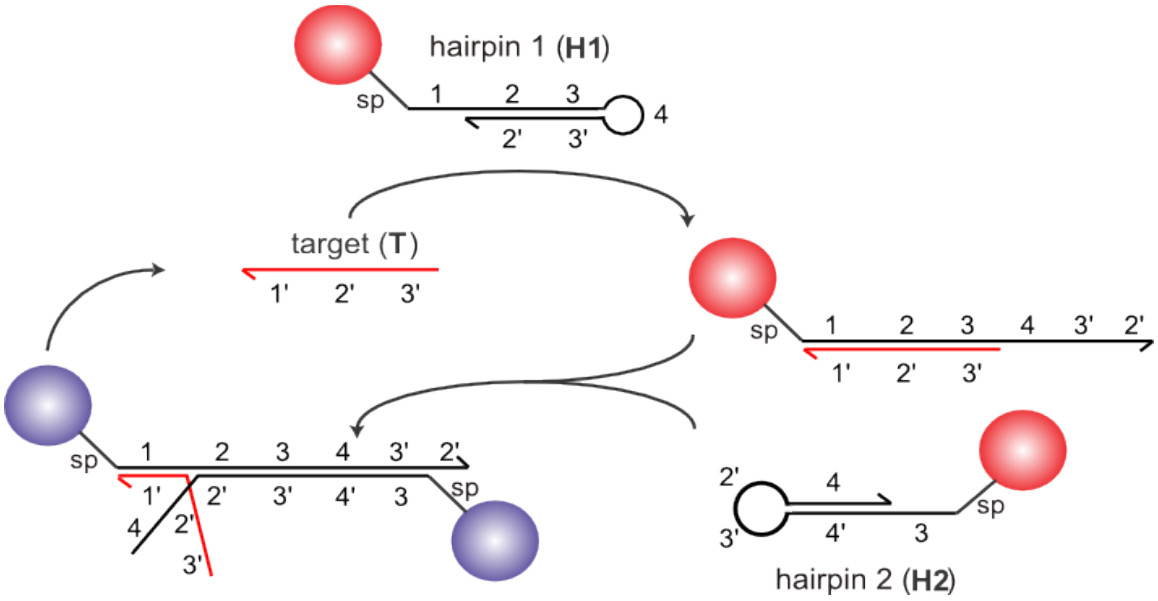

Figure 4.2 Mechanism for Colorimetric Detection with CHA. This naive approach simply aimed to attach nanoparticles onto the hairpins from the original CHA reaction. As the hairpins catalytically hybridize, NP aggregation should occur.

The nanoparticle aggregation results, however, showed less catalytic activity. The gold nanoparticles were loaded with up to 500 strands per particle using the standard procedure and then mixed together with several target concentrations. The data is not shown because there was no significant aggregation at any concentration. It is suspected that the dense loading of hairpins onto the nanoparticle surface can cause steric hindrance for the strand displacement process (Figure 4.4). As such, several designs and procedural modifications were devised for the CHA system.

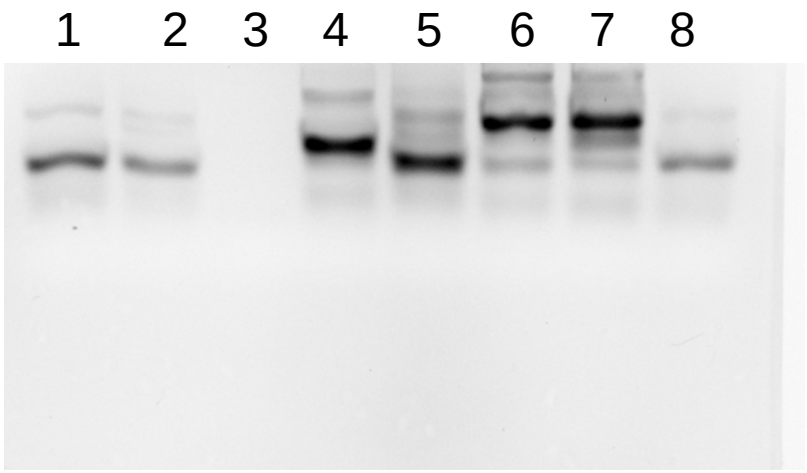

Lane 1:H1
Lane 2: H2
Lane 3: T
Lane 4: H1 + T
Lane 5: H1 + H2
Lane 6: H1 + H2 + 0.2x T
Lane 7: H1 + H2 + 1x T
Lane 8: H2 + T

1x = 1 μM DNA concentration

Figure 4.3 CHA Reaction Products in Gel Electrophoresis. The two hairpins in the test solution are metastable since the band in lane 5 is basically a superposition of the two bands in lanes 1 and 2 (ignoring slight deformation of the bands on the left of the gel). The target strand does bind to H1, forming a larger complex. An even larger complex is formed by the fully operating system in lanes 6 and 7, and this complex is speculated to be the hairpin dimer. Note that lane 6 forms essentially the same amount of this large product as lane 7 and both consume almost all of their hairpin reagents even though the reaction in lane 6 is triggered with sub-stoichiometric amounts of the target strand. This supports the notion that the target strand behaves catalytically for the dimerization of the hairpins.

Design Two: 3' Attachment

Our goal in this design was to reduce steric hindrance at what is suspected to be the rate-limiting binding event. The mechanism shown in Figure 4.2 can be considered to proceed in 3 steps. The first step requires the target strand to bind to the toehold on hairpin 1. Since the hairpin 1 strand is densely packed on the nanoparticle surface, it is more difficult for the target to diffuse past the double-stranded layer than it would in the case of singular free-floating hairpins (Fig. 4.4). This alone could reduce the reaction rate considerably, but the steric hindrance would be even more severe at the second step of

the mechanism. In the second step, the target/hairpin 1 complex includes a long double-stranded region that must penetrate through the densely packed double-stranded layer surrounding the second nanoparticle. The third step in the mechanism involves dissociation events and is therefore not considered to be dramatically hindered by

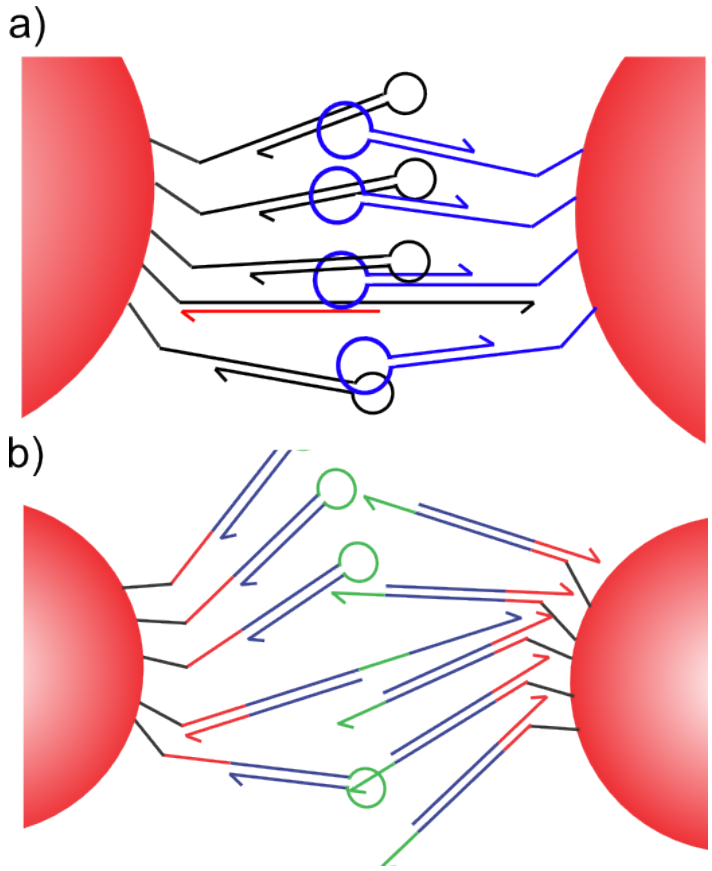

Figure 4.4 DNA Crowding on NP Surface. a) In order for the hairpins on the two nanoparticle types of CHA to align their complimentary toehold domains, the activated hairpin 1 must penetrate the crowded field of DNA on the other nanoparticle and reach the toehold of hairpin 2 that is close the nanoparticle surface. Because of this, there is significant overlap between the DNA fields of the two nanoparticles, even for the adjacent strands not participating in the reaction. This overlap causes DNA to DNA steric hindrance that prevents proper alignment. b) By contrast, the toehold on the linker/target complex in the HCR-based designs from Chapter Two are on the distal end of complex relative to the nanoparticle. In order for the hairpin and linker/target complex to align, there does not need to be as much overlap between the crowded DNA fields of the two nanoparticles, allowing for easier approach.

crowding. We therefore considered the second step to be most rate-limiting and in need of modification. Our solution was to move the spacer and the nanoparticle-binding thiol to the 3' end of hairpin 2. This moves the binding site for the target/hairpin 1 complex to the distal end outside of the densely packed hairpin 2 layer (Figure 4.5).

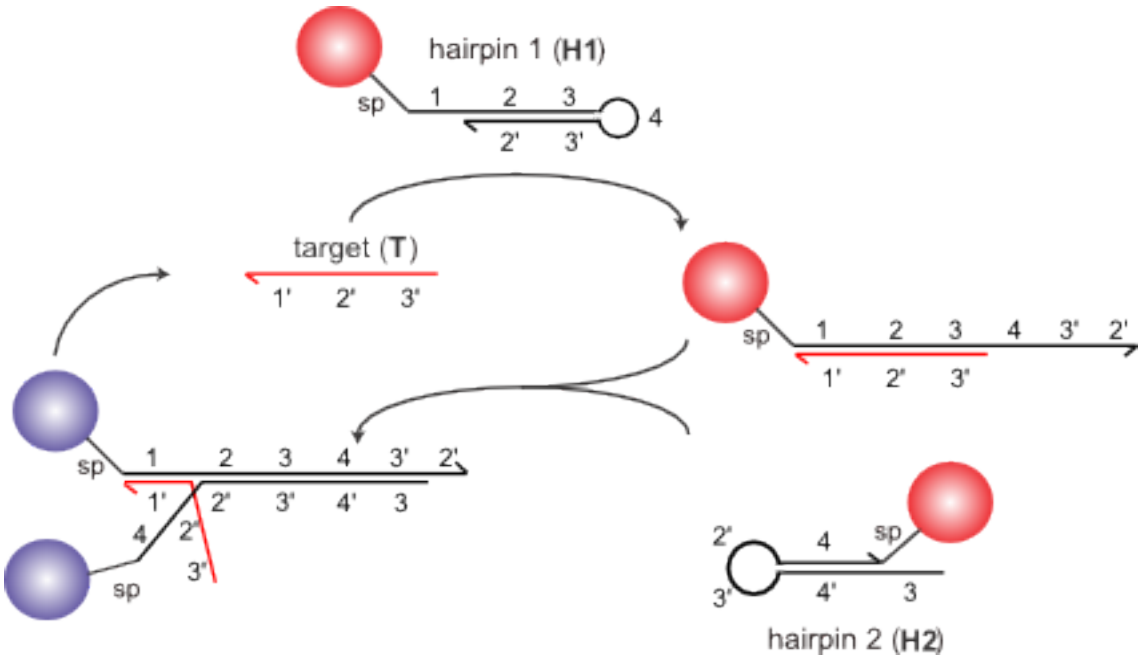

Figure 4.5 CHA Design Two. This version of the CHA-based nanoparticle aggregation design used a modified hairpin 2 strand with the attachment site for the nanoparticle on the 3' end of the strand rather than the 5' end. The spacer region was also moved and elongated. After nanoparticle aggregation, the resulting bridge is in a different orientation than the bridge in CHA design 1.

While this alteration makes the toehold on hairpin 2 more open, it is not necessarily more accessible since it is now at an unfavorable orientation when it binds to hairpin 1 and would force the nanoparticles closer together as strand displacement progresses. To alleviate this latter effect and to maintain a comparable inter-particle distance with our first CHA design, the spacer region was lengthened to 30 thymines. Nanoparticles with the new hairpin 2 were functionalized, mixed with the hairpin 1

nanoparticles and tested with various concentrations of the target. The system was still not capable of aggregation. This result prompted us to adopt a more elaborate modification.

Design Three: Tethered Hairpin 2

In both HCR and CHA, the gel electrophoresis results suggest greater catalytic potential than seen with the aggregation experiments after the strands were attached to nanoparticles. This observation prompted a design whereby the free hairpins are first allowed to react with each other, catalyzed by the target strand, and then attached to the nanoparticles. There are technical difficulties with simply leaving the hairpin strands in a reduced thiol state during the stand-displacement reactions and then adding nanoparticles later, since non-functionalized particles are not stable in the DNA reaction buffer. However, by replacing the spacer region on the hairpin with a tether sequence, which will be complimentary to a tether that is functionalized on a nanoparticle, we provide an alternate form of attachment between hairpins and NPs that can be formed after the CHA reaction has run its course. In this design, only the hairpin 2 was modified with a tether sequence rather than a thiol, and hairpin 1 remains anchored to a nanoparticle (Figure 4.6). After the hairpin 1 functionalized particles, hairpin 2, and target have incubated for a given time, we then add the complimentary tether functionalized particles. If the target successfully induces CHA, then hairpin 1 and hairpin 2 will be hybridized, and the tether functionalized particles with be hybridized to hairpin 2, forming an indirect bridge between nanoparticles.

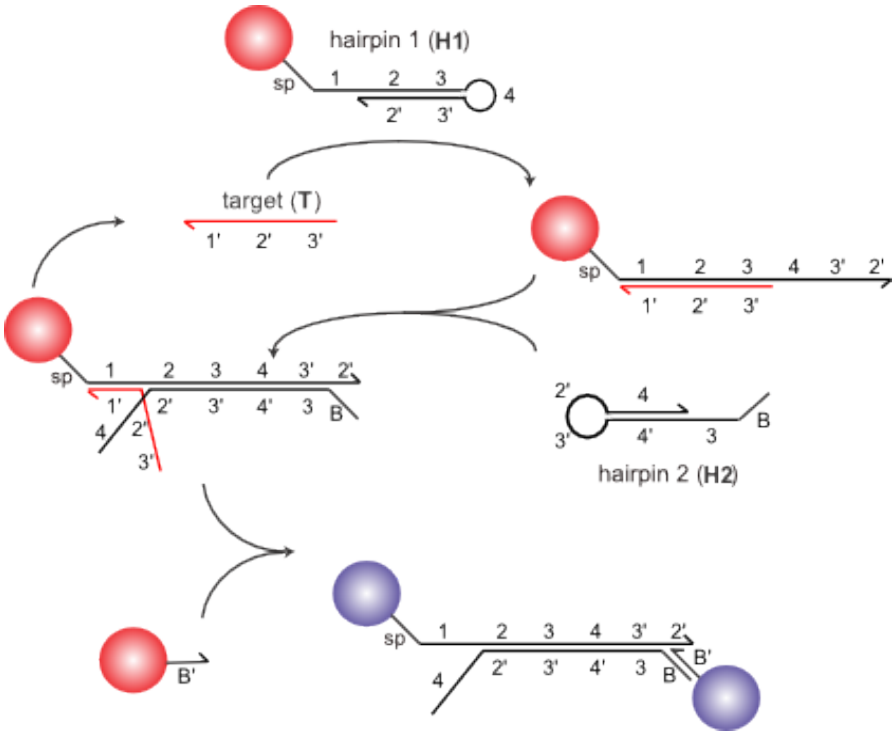

Figure 4.6 Mechanism of the Tethered Design. In this version, the CHA reaction between hairpin-1-bound particles and free-floating hairpin 2 is allowed to proceed first and only after a set incubation time are the nanoparticles with the probe for hairpin 2 added to the solution for colorimetric readout.

Up until now we have only altered the orientations of domains and the lengths of repetitive domains, and no specific domain sequences were altered (Table A.1). In order to introduce the tether sequence, which is a domain not present in the original study by Li *et al.*, we must ensure that the new domain is compatible with the other functional domains. Compatibility implies that the new strand does not bind to and competitively inhibit other binding domains and thus we quantify predicted compatibility by the estimated binding energy of the new sequence to others. This process can be automated by hybridization simulating software like NUPACK, which contains a "design" feature whereby existing domains sequences are specified, domain orientations are defined and

the program optimizes a sequence for your new domain of a specified length such that alternate secondary structure is minimized [46].

Note that our procedure from the last two experiments has to be modified somewhat for this design. Normally, we functionalize one set of nanoparticles with thiolated hairpin 1 and another set with thiolated hairpin 2 then combine them and add the target. For this design, we instead functionalized only the first set of nanoparticles with hairpin 1 and functionalized the second with the tether strand. The CHA reaction was run without the tether-functionalized particles by simply using the hairpin 1-functionalized particles, free hairpin 2 strands with tether binding domains, and target strand. After a given reaction time for CHA to proceed, we then added the tether-functionalized particles so as to produce the optical readout. If the target induced significant rounds of CHA reaction, then each hairpin 1 functionalized particle would be coated with hairpin 2 strand, which has the binding domain to the other nanoparticle and aggregation would occur. If CHA was not triggered because there was a lack of target, then the hairpin 2 would bind to the tether-functionalized particles, but hairpin 2 would not be attached to hairpin 1 and there would be no binding between nanoparticles. This project is still at an earlier phase in its development than the HCR-based designs of Chapter Two, so only the peak shift was measured for these reactions.

This design produced significant aggregation. The first experiment used a 24-hour incubation for the CHA reaction, then 48 additional hours after adding the tether particles. The results are shown in Figure 4.7. The negative control is stable with no detectible peak shift. Low concentrations of the target produce increasing levels of peak

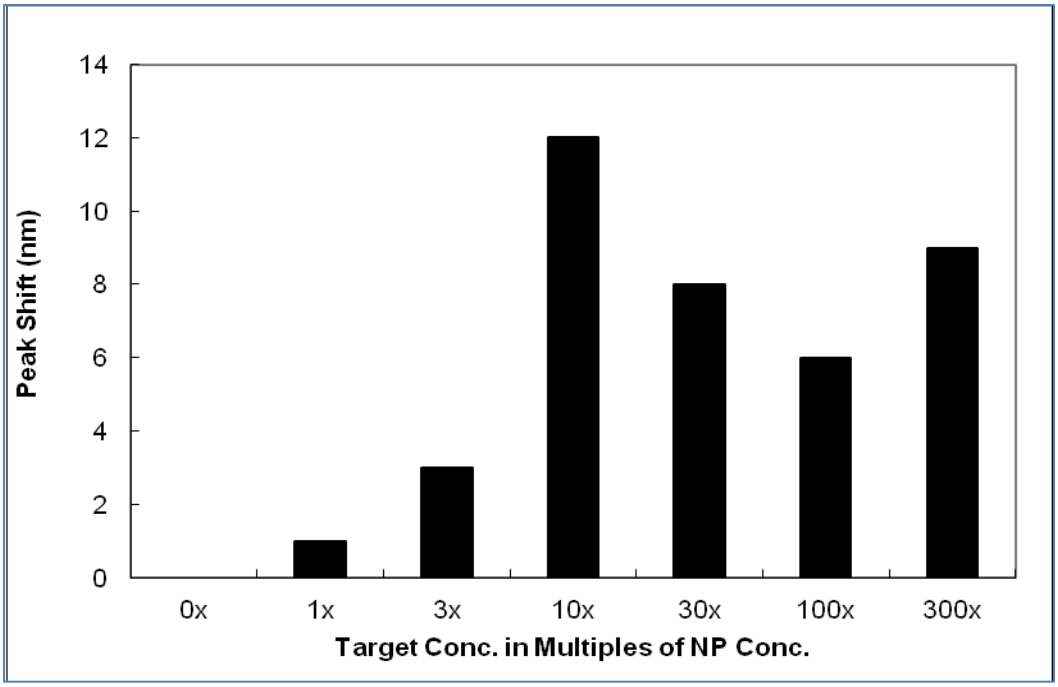

Figure 4.7 Aggregation Results for Tether CHA Design. The correlation between target concentration and peak shift holds between 0x and 10x target, but the correlation becomes disturbed at higher concentrations, presumably due to binding of the 3' domain of the target to the 3 domain of hairpin 2. Still, the fact that this system aggregates at all makes it a dramatic improvement over the previous two designs, and the fact that there is measurable peak shift in the 3x and 1x reaction yet none in the negative control suggest that CHA has potential to be much more sensitive than direct aggregation and also more stable than HCR-based designs.

shift up until the 30x target concentration, which exhibited lower peak shift than the 10x The fact that target concentrations higher than 10x produced less aggregation than the 10x was presumed to be experimental error at first, but the results were reproduced, and then reproduced two more times by another individual in our lab. In each case, the 10x reaction had the highest peak shift. This behavior indicates that there may be a threshold beyond which the target strand starts to inhibit the reaction. Looking at the domain-level design is possible that the 3' domain of the target strand is transiently binding to the 3 domain on hairpin 2. Because the target strand does not possess the 4 domain, it can't perform toehold-mediated strand displacement on hairpin 2, but if there is enough target

strands in solution, then a large portion of the hairpin 2 strands may be bound to target and would then be unavailable for binding with the activated hairpin 1 as intended.

Future Work

Further efforts on this project should include measurements at different time-points and the inclusion of target concentrations of 100x and higher to determine if the aggregation truly plateaus with respect to target is inhibited by too much target, or eventually increases. If it is verified that too much target inhibits the reaction by binding to hairpin 2, then a possible solution would be to introduce mismatch point mutations into the target strand. Such point mutations would make the target slightly less efficient at opening hairpin 1, but they would be expected to decrease the rate of binding to hairpin 2 much more. Using point mutations to adjust the relative reaction rates of unfavorable and favorable reactions has already been explored by the same lab that developed the CHA reaction originally [71]. In a real diagnostic design, the target strand has biological relevance and should not be altered, thus requiring the hairpins to be altered instead, but the reaction is still in the proof-of-concept stage with non-biologically-relevant sequences.

Eventually, we would also like to test two related designs: one in which hairpin 2 is attached to the nanoparticle and hairpin 1 is free-floating and contains a tether sequence, and another design in which both hairpins are free-floating and contain different tether sequences such that CHA is first reacted in the absence of nanoparticles. Our prediction is that the design with just hairpin 2-coated nanoparticles and free hairpin 1 will aggregate less efficiently than the experiment of Figure 4.7 because, if you recall, it

is the step in which hairpin 1/target complex binds to hairpin 2 that we predict to be the most rate-limiting.

Catalytic hairpin assembly shows great promise as an amplification reaction for nanoparticle-based colorimetric detection. Modifications from the original design were needed to overcome the steric hindrance associated with attaching the hairpins to nanoparticle surfaces. With such modifications, this amplification scheme exhibits lower detection limits than conventional, direct nanoparticle aggregation. Furthermore, CHA offers several features that render it more favorable than HCR for the purposes of incorporation with nanoparticles. Unlike HCR, CHA can be considered truly catalytic because each cycle of the mechanism releases the original target strand back into solution, which bypasses the leakage associated with pre-treating the HCR particles with the target strand. CHA also inherently forms many dimers of hairpins as opposed to the long, alternating polymer of hairpins formed in the original HCR design and this is favorable because the dimers translate to discrete bridges between nanoparticles, which is less sterically hindered than the linear array of nanoparticles formed by our first adaptation of HCR. These advantages make CHA a promising alternative, but now that we have a better understanding of what makes a given amplification network ideal for nanoparticles, we might select an even better network from those that are being published lately or perhaps develop a new DNA reaction network tailored from the beginning for use with nanoparticles.

CHAPTER FIVE: CONCLUSION

A Summary and Perspectives

We set out to create a low-cost, reliable and field-deployable test that could be used to detect DNA sequences and other biomolecules at very low concentrations. To make the test simple to operate for the end user, we adopted the color-changing capability of gold colloids as they aggregate. Gold colloids are preferable to organic dye-based indicators because their higher extinction coefficient renders them capable of producing a strong visual response, even at lower analyte concentrations without requiring any more instrumentation than organic dyes. Even gold NPs, though, have their limits. Some researchers have found ways to improve the detection limit for gold NP-based bioassays, though it is typically at the expense of simplicity for the user and often requires advanced instrumentation or several post-treatments after reacting with the test sample.

For oligonucleotide targets, the effective concentration can be increased using a DNA reaction network. These amplification networks are difficult to engineer and troubleshoot, but unlike the more popular PCR reaction, they do not require enzymes or a thermocycler and are thus easier to use by an untrained person in the field once the components have been mixed in a lab. As such, we enhanced NP-based colorimetric tests by incorporating DNA amplification networks. The first such network used was Hybridization Chain Reaction, which required severe modifications in order to overcome the crowding problems associated with binding so many hairpins to each nanoparticle.

HCR was also used with an aptamer transducer, which allowed us to detect adenosine via the amplification network. Finally, we employed another amplification design, Catalytic Hairpin Assembly, with our nanoparticles, which also had issues with steric hindrance, but ultimately was able to detect lower concentrations of DNA than direct NP aggregation designs.

So did we achieve our goal of producing a cheap, reliable and easy field test? Not to completion. We did, however, make great strides towards this goal. We've provided evidence that our combination of gold nanoparticles and DNA amplification has improved detection limits over using direct nanoparticle aggregation alone. In most cases, this increase was only about three to tenfold, less that we had hoped for, but still potentially significant and there is still room for optimization. But what of our three criteria?

Is the test simple? The nanoparticles functionalized with hairpin or linker/target complexes can be prepared in the lab and will remain active for about a month. All the end user needs to do is combine the two nanoparticle types and add their sample. This sounds simple enough at first, but so far we have only used "samples" of the same buffer and containing only one or two sequences. Tests will need to be performed to see if samples such as blood or cheek swabs will need to be purified beforehand, which would complicate the test.

Is the test reliable? Reproducibility was an issue with some of the faulty designs but is generally reasonable and comparable to direct NP aggregation as evident by the error bars seen in the graphs of Chapter Two.

Is the assay cheap? The primary costs of producing the nanoparticles come from three sources. First, there are the synthetic DNA oligonucleotides used to functionalize the nanoparticles, but synthetic DNA is becoming ever more efficiently produced. Second there is the colloidal gold, which sounds very expensive to those not used to working with it. It is gold after all, but the concentrations needed are so low thanks to high extinction coefficient of gold NPs. Just a few milligrams of chloroauric acid are sufficient for hundreds to thousands of our reactions, each of which is large enough for the color change to be visibly detectible. Finally, there is the labor cost, which is relatively high for bench-scale academic research, but would become much cheaper if the tests are ever mass produced.

In short, this project still has great potential to help the fields of medicine and field research. Even though I will not be continuing to work on this project personally, the torch has been passed to other students who are currently working to optimize the CHA and aptamer designs in particular.

APPENDIX A

Materials and Sequences

Table A.1 DNA Sequences Used

Chapter 1		
Design	Name	Sequence
HCR	Hairpin 1 (H1)	5'-/TTAACCCACGCCGAATCCTAGACTCAAAGTAG TCTAGGATTCGGCGTG-3'
	Hairpin 2 (H2)	5'-/AGTCTAGGATTCGGCGTGGGTTAACACGCCGA ATCCTAGACTACTTTG/-3'
	Target (T)	5'-/AGTCTAGGATTCGGCGTGGGTTAA-3'
Chapter 2		
Design	Name	Sequence
Design 1	Probe 1	5'-/thiol/TTTTTTTTTTTTCGTAGGAGCACTGGT-3'
	Probe 2	5'-CGTAGGCGGTAGAGATTTTTTTTTTT/thiol/-3
	Target (T)	5'-TCTCTACCGCCTACGACCAGTGCTCCTACG-3'
Design 2	Hairpin 1 (H1)	5'-/thiol/TTTTTTTTTTTTTTAACCCACGCCGAATCCT AGACTCAAAGTAGTCTAGGATTCGGCGTG-3'
	Hairpin 2 (H2)	5'-/AGTCTAGGATTCGGCGTGGGTTAACACGCCGA ATCCTAGACTACTTTGTTTTTTTTTTTT/thiol/-3'
	Target (T)	5'-/AGTCTAGGATTCGGCGTGGGTTAA-3'
	Hairpin (H)	5'-/thiol/TTTTTTTTTTTTTTAACCCACGCCGAATCCT AGACTCAAAGTAGTCTAGGATTCGGCGTG-3'

Design 3	Linker (L)	5'-/thiol/TTTTTTTTTTTTCACGCCGAATCCTAGACTACTTTG-3'
	Target (T)	5'-/AGTCTAGGATTCGGCGTGGGTTAA-3'
Design 4	Hairpin (H)	5'-/thiol/TTTTTTTTTTTTTTAACCCACGCCGAATCCTAGACTCAAAGTAGTCTAGGATTCGGCGTG-3'
	Linker (L)	5'-/thiol/TTTTTTTTTTTTACCCACGCCGAATCCTAGACTACTTTG-3’
	Target (T)	5'-/AGTCTAGGATTCGGCGTGGGTTAA-3'
Design 5	Hairpin (H)	5'-/thiol/TTTTTTAACCCACGCCTAGACTCAAAGTAGTCTAGGCGTG-3'
	Linker (L)	5'-/thiol/TTTTACCCACGCCTAGACTACTTTG-3'
	Target (T)	5'-/AGTCTAGGCGTGGGTTAA-3'
Chapter 3		
Design	Name	Sequence
	Hairpin (H)	5'-/ TAACAAGAAAGCCAAACCGAGATGGGT TTGGCTTTCTTGTTACCTGGGTTTTTTTTTTTT/thiol/-3'
	Linker (L)	5'-/CATCTCGGTTTGGCTTTCTTGTTACCTTTTTTTTTTTTT/thiol/-3'
	Signal (S)	5'-/CCCAGGTAACAAGAAAGCCAAACC-3'
	Transducer (Trn)	5'-/CCCAGGTAACAAGAAAGCCAAACC TCTTGTTACCTGGGGGAGTATTGCGGAGGAAGGT-3'
Chapter 4		
Design	Name	Sequence
Design 1	Hairpin 1 (H1)	5'-/thiol/TTTTTTTTTTTTGTCAGTGAGCTAGGTTAGATGTCGCCATGTGTAGACGACATCTAACCTAGC/-3'
	Hairpin 2 (H2)	5'-/thiol/TTTTTTTTTTTTAGATGTCGTCTACACATGGCGACATCTAACCTAGCCCATGTGTAGA/-3'

	Target (T)	5'-/CGACATCTAACCTAGCTCACTGAC/-3'
Design 2	Hairpin 1 (H1)	5'-/thiol/TTTTTTTTTTTTGTCAGTGAGCTAGGTTAGA TGTCGCCATGTGTAGACGACATCTAACCTAGC/-3'
	Hairpin 2 (H2)	5'-/AGATGTCGTCTACACATGGCGACATCTAACCTA GCCCATGTGTAGATTTTTTTTTTTTTTTTTTTTTTT TTTTTTTTTT/thiol/-3'
	Target (T)	5'-/CGACATCTAACCTAGCTCACTGAC/-3'
Design 3	Hairpin 1 (H1)	5'-/thiol/TTTTTTTTTTTTGTCAGTGAGCTAGGTTAGA TGTCGCCATGTGTAGACGACATCTAACCTAGC/-3'
	Hairpin 2 (H2)	5'-/AGTTTAGTTTCCAGATGTCGTCTACACATGG CGACATCTAACCTAGCCCATGTGTAGA/-3'
	Target (T)	5'-/CGACATCTAACCTAGCTCACTGAC/-3'
	Tether	5'-/GGAAACTAAACT/thiol/-3'

REFERENCES

1. Kirsch, J., et al., *Biosensor technology: recent advances in threat agent detection and medicine.* Chemical Society Reviews, 2013. **42**(22): p. 8733-8768.
2. Sandhu, H. and H. Maddock, *Molecular basis of cancer-therapy-induced cardiotoxicity: introducing microRNA biomarkers for early assessment of subclinical myocardial injury.* Clinical Science, 2014. **126**(5-6): p. 377-400.
3. Hoa, X.D., A.G. Kirk, and M. Tabrizian, *Towards integrated and sensitive surface plasmon resonance biosensors: A review of recent progress.* Biosensors and Bioelectronics, 2007. **23**(2): p. 151-160.
4. Han, S.-X., et al., *Molecular Beacons: A Novel Optical Diagnostic Tool.* Archivum Immunologiae et Therapiae Experimentalis, 2013. **61**(2): p. 139-148.
5. Rolfs, A., et al., *PCR: clinical diagnostics and research*. 1992: Springer-Verlag Berlin.
6. Kumar, S., et al., *Microfluidic-integrated biosensors: Prospects for point-of-care diagnostics.* Biotechnology Journal, 2013. **8**(11): p. 1267-1279.
7. Elghanian, R., et al., *Selective colorimetric detection of polynucleotides based on the distance-dependent optical properties of gold nanoparticles.* Science, 1997. **277**(5329): p. 1078-1081.
8. Medley, C.D., et al., *Gold nanoparticle-based colorimetric assay for the direct detection of cancerous cells.* Analytical chemistry, 2008. **80**(4): p. 1067-1072.
9. Kim, Y., R.C. Johnson, and J.T. Hupp, *Gold nanoparticle-based sensing of "spectroscopically silent" heavy metal ions.* Nano Letters, 2001. **1**(4): p. 165-167.
10. Nam, J.-M., C.S. Thaxton, and C.A. Mirkin, *Nanoparticle-based bio-bar codes for the ultrasensitive detection of proteins.* Science, 2003. **301**(5641): p. 1884-1886.
11. Thanh, N.T.K. and Z. Rosenzweig, *Development of an aggregation-based immunoassay for anti-protein A using gold nanoparticles.* Analytical chemistry, 2002. **74**(7): p. 1624-1628.
12. Homola, J., S.S. Yee, and G. Gauglitz, *Surface plasmon resonance sensors: review.* Sensors and Actuators B: Chemical, 1999. **54**(1): p. 3-15.
13. Atay, T., J.-H. Song, and A.V. Nurmikko, *Strongly interacting plasmon nanoparticle pairs: from dipole-dipole interaction to conductively coupled regime.* Nano Letters, 2004. **4**(9): p. 1627-1631.
14. Ghosh, S.K. and T. Pal, *Interparticle coupling effect on the surface plasmon resonance of gold nanoparticles: from theory to applications.* Chem Rev, 2007. **107**(11): p. 4797-862.
15. Pattnaik, P., *Surface plasmon resonance.* Applied biochemistry and biotechnology, 2005. **126**(2): p. 79-92.
16. Mayer, K.M. and J.H. Hafner, *Localized Surface Plasmon Resonance Sensors.* Chemical Reviews, 2011. **111**(6): p. 3828-3857.

17. Hu, M., et al., *Gold nanostructures: engineering their plasmonic properties for biomedical applications.* Chemical Society Reviews, 2006. **35**(11): p. 1084-1094.
18. Zhao, W., et al., *Simple and rapid colorimetric biosensors based on DNA aptamer and noncrosslinking gold nanoparticle aggregation.* ChemBioChem, 2007. **8**(7): p. 727-731.
19. Kim, T., et al., *Kinetics of gold nanoparticle aggregation: experiments and modeling.* Journal of colloid and interface science, 2008. **318**(2): p. 238-243.
20. Storhoff, J.J., et al., *What controls the optical properties of DNA-linked gold nanoparticle assemblies?* Journal of the American Chemical Society, 2000. **122**(19): p. 4640-4650.
21. Liz-Marzán, L.M., M. Giersig, and P. Mulvaney, *Synthesis of nanosized gold-silica core-shell particles.* Langmuir, 1996. **12**(18): p. 4329-4335.
22. Castañeda, M.e.T., S. Alegret, and A. Merkoci, *Electrochemical sensing of DNA using gold nanoparticles.* Electroanalysis, 2007. **19**(7‐8): p. 743-753.
23. Bunz, U.H. and V.M. Rotello, *Gold nanoparticle–fluorophore complexes: sensitive and discerning "noses" for biosystems sensing.* Angewandte Chemie International Edition, 2010. **49**(19): p. 3268-3279.
24. Zhang, S., et al., *Covalent attachment of glucose oxidase to an Au electrode modified with gold nanoparticles for use as glucose biosensor.* Bioelectrochemistry, 2005. **67**(1): p. 15-22.
25. Dirks, R.M. and N.A. Pierce, *Triggered amplification by hybridization chain reaction.* Proceedings of the National Academy of Sciences of the United States of America, 2004. **101**(43): p. 15275-15278.
26. Paukstelis, P.J., et al., *Crystal structure of a continuous three-dimensional DNA lattice.* Chemistry & biology, 2004. **11**(8): p. 1119-1126.
27. Winfree, E., et al., *Design and self-assembly of two-dimensional DNA crystals.* Nature, 1998. **394**(6693): p. 539-544.
28. Tørring, T., et al., *DNA origami: a quantum leap for self-assembly of complex structures.* Chemical Society Reviews, 2011. **40**(12): p. 5636-5646.
29. Ding, B., et al., *Gold nanoparticle self-similar chain structure organized by DNA origami.* Journal of the American Chemical Society, 2010. **132**(10): p. 3248-3249.
30. Zhang, D.Y. and E. Winfree, *Control of DNA Strand Displacement Kinetics Using Toehold Exchange.* Journal of the American Chemical Society, 2009. **131**(47): p. 17303-17314.
31. Panyutin, I.G. and P. Hsieh, *The kinetics of spontaneous DNA branch migration.* Proceedings of the National Academy of Sciences, 1994. **91**(6): p. 2021-2025.
32. Srinivas, N., et al., *On the biophysics and kinetics of toehold-mediated DNA strand displacement.* (1362-4962 (Electronic)).
33. Ellwood, M., et al., *Strand displacement applied to assays with nucleic acid probes.* Clinical chemistry, 1986. **32**(9): p. 1631-1636.
34. Johnson, D.A., et al., *Improved technique utilizing nonfat dry milk for analysis of proteins and nucleic acids transferred to nitrocellulose.* Gene Analysis Techniques, 1984. **1**(1): p. 3-8.
35. Doherty, E.A. and J.A. Doudna, *Ribozyme structures and mechanisms.* Annual review of biochemistry, 2000. **69**(1): p. 597-615.

36. Reynolds, A., et al., *Rational siRNA design for RNA interference.* Nature biotechnology, 2004. **22**(3): p. 326-330.
37. Nudler, E. and A.S. Mironov, *The riboswitch control of bacterial metabolism.* Trends in biochemical sciences, 2004. **29**(1): p. 11-17.
38. Okamoto, A., K. Tanaka, and I. Saito, *DNA logic gates.* Journal of the American Chemical Society, 2004. **126**(30): p. 9458-9463.
39. Willner, I., et al., *DNAzymes for sensing, nanobiotechnology and logic gate applications.* Chemical Society Reviews, 2008. **37**(6): p. 1153-1165.
40. Seelig, G., et al., *Enzyme-free nucleic acid logic circuits.* science, 2006. **314**(5805): p. 1585-1588.
41. Bath, J. and A.J. Turberfield, *DNA nanomachines.* Nature nanotechnology, 2007. **2**(5): p. 275-284.
42. Yurke, B., et al., *A DNA-fuelled molecular machine made of DNA.* Nature, 2000. **406**(6796): p. 605-608.
43. Lubrich, D., J. Lin, and J. Yan, *A contractile DNA machine.* Angewandte Chemie International Edition, 2008. **47**(37): p. 7026-7028.
44. Qian, L. and E. Winfree, *A simple DNA gate motif for synthesizing large-scale circuits.* Journal of The Royal Society Interface, 2011. **8**(62): p. 1281-1297.
45. Zhang, D.Y., et al., *Engineering entropy-driven reactions and networks catalyzed by DNA.* Science, 2007. **318**(5853): p. 1121-1125.
46. Zadeh, J.N., et al., *NUPACK: analysis and design of nucleic acid systems.* Journal of computational chemistry, 2011. **32**(1): p. 170-173.
47. Beebe, T.P. and C.E. Rabke-Clemmer, *Thiol labeling of DNA for attachment to gold surfaces*. 1995, Google Patents.
48. Kimling, J., et al., *Turkevich method for gold nanoparticle synthesis revisited.* The Journal of Physical Chemistry B, 2006. **110**(32): p. 15700-15707.
49. Anderson, C.F. and M.T. Record Jr, *Polyelectrolyte theories and their applications to DNA.* Annual Review of Physical Chemistry, 1982. **33**(1): p. 191-222.
50. Leal, C., et al., *Electrostatic attraction between DNA and a cationic surfactant aggregate. The screening effect of salt.* The Journal of Physical Chemistry B, 2007. **111**(21): p. 5999-6005.
51. Hurst, S.J., A.K. Lytton-Jean, and C.A. Mirkin, *Maximizing DNA loading on a range of gold nanoparticle sizes.* Analytical chemistry, 2006. **78**(24): p. 8313-8318.
52. Park, S.-J., et al., *The structural characterization of oligonucleotide-modified gold nanoparticle networks formed by DNA hybridization.* The Journal of Physical Chemistry B, 2004. **108**(33): p. 12375-12380.
53. Jain, P.K., W. Huang, and M.A. El-Sayed, *On the universal scaling behavior of the distance decay of plasmon coupling in metal nanoparticle pairs: a plasmon ruler equation.* Nano Letters, 2007. **7**(7): p. 2080-2088.
54. Watson, J.D. and F.H. Crick, *Molecular structure of nucleic acids.* Nature, 1953. **171**(4356): p. 737-738.
55. Markham, N.R. and M. Zuker, *DINAMelt web server for nucleic acid melting prediction.* Nucleic acids research, 2005. **33**(suppl 2): p. W577-W581.

56. Lee, O.-c., J.-H. Jeon, and W. Sung, *How double-stranded DNA breathing enhances its flexibility and instability on short length scales.* Physical Review E, 2010. **81**(2): p. 021906.
57. Bois, J.S., et al., *Topological constraints in nucleic acid hybridization kinetics.* Nucleic acids research, 2005. **33**(13): p. 4090-4095.
58. Green, S.J., D. Lubrich, and A.J. Turberfield, *DNA hairpins: fuel for autonomous DNA devices.* Biophysical journal, 2006. **91**(8): p. 2966-2975.
59. Kim, M.G., et al., *Probing the structure of a putative intermediate in homologous recombination: the third strand in the parallel DNA triplex is in contact with the major groove of the duplex.* Journal of molecular biology, 1995. **247**(5): p. 874-889.
60. Lin, C.H. and D.J. Patei, *Structural basis of DNA folding and recognition in an AMP-DNA aptamer complex: distinct architectures but common recognition motifs for DNA and RNA aptamers complexed to AMP.* Chemistry & biology, 1997. **4**(11): p. 817-832.
61. Brody, E.N. and L. Gold, *Aptamers as therapeutic and diagnostic agents.* Reviews in Molecular Biotechnology, 2000. **74**(1): p. 5-13.
62. Greenleaf, W.J., et al., *Direct observation of hierarchical folding in single riboswitch aptamers.* Science, 2008. **319**(5863): p. 630-633.
63. Zhang, Q., X.J. Liu, and Y. Liu, *Aptamers as Recognition Elements for Analysis of Small Molecules.* Asian Journal of Chemistry, 2012. **24**(1): p. 1-6.
64. Stoltenburg, R., C. Reinemann, and B. Strehlitz, *SELEX—a (r) evolutionary method to generate high-affinity nucleic acid ligands.* Biomolecular engineering, 2007. **24**(4): p. 381-403.
65. HUIZENGA, D. and J. SZOSTAK, *A DNA APTAMER THAT BINDS ADENOSINE AND ATP.* Biochemistry, 1995. **34**(2): p. 656-665.
66. Goda, T. and Y. Miyahara, *A hairpin DNA aptamer coupled with groove binders as a smart switch for a field-effect transistor biosensor.* Biosensors & Bioelectronics, 2012. **32**(1): p. 244-249.
67. Wang, J., et al., *A Gold Nanoparticle‐Based Aptamer Target Binding Readout for ATP Assay.* Advanced Materials, 2007. **19**(22): p. 3943-3946.
68. Huang, C.-C., et al., *Aptamer-modified gold nanoparticles for colorimetric determination of platelet-derived growth factors and their receptors.* Analytical chemistry, 2005. **77**(17): p. 5735-5741.
69. Liu, J. and Y. Lu, *Fast colorimetric sensing of adenosine and cocaine based on a general sensor design involving aptamers and nanoparticles.* Angewandte Chemie, 2006. **118**(1): p. 96-100.
70. Li, B., A.D. Ellington, and X. Chen, *Rational, modular adaptation of enzyme-free DNA circuits to multiple detection methods.* Nucleic acids research, 2011. **39**(16): p. e110-e110.
71. Jiang, Y.S., et al., *Mismatches improve the performance of strand-displacement nucleic Acid circuits.* Angew Chem Int Ed Engl, 2014. **53**(7): p. 1845-8.